5-2015

Syntheses, Structures and Properties of Metal-Organic Frameworks

Xin Liu
Western Kentucky University, xin.liu261@topper.wku.edu

SYNTHESES, STRUCTURES AND PROPERTIES OF METAL-ORGANIC FRAMEWORKS

A Thesis
Presented to
The Faculty of the Department of Chemistry
Western Kentucky University
Bowling Green Kentucky

In Partial Fulfillment
of the Requirement for the Degree
Master of Science

Xin Liu

May, 2015

SYNTHESEIS, STRUCTURES, AND PROPERTIES OF METAL-ORGANIC FRAMEWORKS

Date Recommended 3/31/2015

Bangbo Yan

Director of Thesis Dr. Bangbo Yan

Dr. Cao Yan

Dr. Darwin Dahl

Dean, Office of Graduate Studies and Research 4-20-15 Date

I dedicate the thesis to my family, to Dr. Bangbo Yan and my friends who supported and encouraged me the most during my challenging but happy times here at Western Kentucky University.

ACKNOWLEDGMENTS

I want to show my deepest gratitude to all of the people who helped me during my whole Master's program period at Western Kentucky University; without their help, my research work and this thesis couldn't be accomplished.

I would like to thank my parents who always give me the right guidance for my life direction and support me always. I want especially to thank my advisor Dr. Bangbo Yan for his patience guidance and everlasting encouragement. In particular, his serious attitude in research guided me greatly.

At the same time, I would like to show my deep appreciation to Dr. Yan Cao and Dr. Darwin Dahl who serve as my thesis committee for their high quality and innovative suggestions, Ms. Alicia McDaniel, for providing chemicals and materials on time, especially for giving me comfort and encouragement when I felt stressed. Thanks to Dr. John Andersland for helping me with SEM and TEM images and Dr. Quentin Lineberry and Mr. William Orndorff who taught me how to operate PXRD and element analysis instrument. I also want to express my gratitude to Dr. Cathleen Webb and Dr. Rajalingam Dakshinamurthy who gave me the right advice in order to accomplish my goals. In addition, I would like to thank my research group members Haley Valentine and Nicholas Fedorka for their help and suggestions.

Last, I want to show my deepest love to my family, my beloved and also the most loyal friend of mine who always can alleviate my anxiety when I faced the stress and without his understanding and support, I couldn't even have the chance to study abroad.

And my lovely precious daughter who always made me feel happiness and feel strong enough to overcome difficulties and insist on my goals. Thanks.

TABLE OF CONTENTS

LIST OF FIGURES

LIST OF TABLES

Page

SYNTHESES, STRUCTURES, AND PROPERTIES OF METAL-ORGANIC FRAMEWORKS

Xin Liu May 2015 Pages 75

Directed By: Bangbo Yan, Cao Yan, and Darwin Dahl

Department of Chemistry Western Kentucky University

Mercury is one of the most serious heavy metal pollution sources that threaten people's health. For decades, people have developed many technologies and materials to capture mercury from flue gas of coal-fired plant. Currently, the most effective material for mercury absorption is powdered activated carbon, which shows increased efficiency when modified with halogen functional groups such as bromine. Metal-organic frameworks (MOFs) have potential applications in mercury capture due to their fantastic properties such as high porosity and high thermal stability. More important, their pore sizes and topology structures can be controlled through choosing different organic ligands in the syntheses. However, their mercury removal properties have not been studied so far. In this project, mercury absorption properties of selected known porous MOFs were studied, and the syntheses of new porous MOFs with functional groups for mercury absorption were investigated.

Three known porous MOFs for mercury sorption properties were investigated. One of these MOFs, compound 3 shows a total efficiency greater than 90% in laboratory scale tests. Moreover, three new MOFs: $[Cu(Br_2BDC)_2](HTEA)_2$, $[Co_2(BrBDC)(HCOO)_2(DMF)_2]$ and $Zn_2(BrBDC)(Trz)_2 \cdot 3H_2O$, (BrBDC = 2,5-dibromoterepthalicate, DMF =dimethylformamide, TEA = trimethylamine,

Trz=1,2,4-triazole) were synthesized successfully. The first two compounds have two-dimensional structures, while the last compound contains three-dimensional channels with opening over 4.7 Å.

CHAPTER I

INTRODUCTION

Mercury has been a notorious environmental pollutant for several decades. It can harm kidneys, livers, and central nervous systems after being absorbed by human beings through different ways. Studies indicated that coal-burning power plants are the main source of mercury pollution, which accounts for about 40% of total mercury emissions in America. In Dec. 2011, the Environmental Protection Agency (EPA) announced a new regulation that requires coal- and oil-fired power plants to control the amount of mercury emission. Their goal is to reduce mercury emissions by approximately 90 percent.[1]

Mercury is mainly found in three forms in coal-derived flue gases: elemental (Hg^0), divalent (Hg^{2+}) and particle-bound $(Hg(p))^2$. For many years, people have developed many different technologies to remove mercury sources, such as air pollution control devices and selective catalytic reduction systems, both of are capable of removing Hg but not at the desired level and mainly target for removal Hg^{2+} and Hg(p) rather than Hg^0.[3] Currently, the most effective material for mercury absorption is powdered activated carbon. Its elemental Hg^0 absorption can be enhanced by impregnating with sulfur and various halogens.[4] However, it has many drawbacks, such as bad performance on for high sulfur coals because of competitive adsorption of sulfur trioxide in coal-fired flue gas.[5] Thus, to develop a new porous material for mercury removal from coal fired power plants is very important. [6]

MOF (metal-organic framework) materials have been known as coordination polymers because they usually form extended structures using organic ligands and metal

ions. Most of the connecting centers in MOF structures are transition metals, which have empty *d* orbitals and can act as acceptors Lewis acid to receive electrons from ligands to form coordination bonds. Extending this kind of structure in three dimensions can generate MOF materials with high porosity. As a class of porous materials, MOFs have attracted extensive attention owing to their high surface area, low densities, high porosity, thermal stability and adjustable chemical functionalities. They have been studied for a variety of applications, such as gas sorption[7], gas separation[8], biomedical applications[9], and catalysis[10].

Many MOFs have been found to exhibit permanent porosity and show pore windows ranging from 5 to 25 Å.[11] MOFs with ultrahigh porosity (up to 90% free volume) and enormous internal surface areas, extending 10000 m^2/g have been synthesized through ligand extension.[6] For example, IRMOF-74-III-CH_2NH_2, can take up CO_2 as high as 3.2 mmol per gram at 800 Torr,[12] MOF-519 has a volumetric methane capacity of 279 cm^3cm^{-3} at 298 K and 80 bar.[13]

Many MOFs have been synthesized containing halogen group through a post-synthesized method.[14] In contrast to this, MOFs impregnated with halogen, such as bromine or chlorine, and synthesized together as one step would appear more convenient and cost effective a method. However, the investigation on the application of MOFs on mercury removal from flue gases has not been reported. In comparison with activated carbon, many MOF parameters such as surface area, pore volume, pore opening can be controlled. In addition, MOFs can be functionalized with many groups such as -Cl, -Br and –COOH, to modify the degree of chemical adsorption as well. The research presented here aims to investigate mercury adsorption performance of selected known

MOFs in simulated flue gases and the synthesis of new MOFs with the intent of testing their mercury absorption ability.

CHAPTER II

Literature Review

2.1. Introduction

Porous materials encompass a broad range of uses in the industrial processes such as absorption and catalysis. Zeolites are quintessential examples among the class of crystalline aluminosilicate materials with interconnected pores of 4~13Å. [15] Compared to zeolites, activated carbons, being an amorphous porous material, have higher porosity and specific surface area and dominate a large part of the solid porous material market.[16]

Metal organic frameworks evolved from coordination and solid-state/zeolite chemistry that were labeled as coordination polymers.[17] They were formed by metal ions as nodes and organic ligands as linkers. Seminal work established by Hoskins and Robson, who set the basis for the future development of MOFs in their paper,[17b, 18] triggered the interest in porous coordination polymers and MOFs around 1990. After that, research on MOFs was popularized by Yaghi [19] et al. especially after MOF-5 was reported. Until now, MOF-5 and Cu-BTC (HKUST-1[20]) were still among the most studied MOFs mainly due to their robust porosity. From 2002, a series of Zn-dicarboxylate MOFs were synthesized and thereby form the concept of isoreticular structure MOFs[21] (IRMOF, $Zn_4O(BDC\text{-}X)_3$, X=Br, NH_2, C_3H_7O), which were prepared by using a variety of 1,4-benzenedicarboxylate acid (BDC) and other elongated dicarboxylate acids with functional groups such as phenols, alkylamines and thiols.[22] With the number MOFs made of single ligands increased, mixed-linker MOFs have

appeared since 2001.[23] The biggest advantage of MOF porous materials is that the number of possible combinations of inorganic and organic components to form resulting structures is incredible and is indeed reflected by the enormous publications from this field in the last two decades.[24] Moreover, MOFs demonstrated unique properties such as magnetism[25] and luminescence[26] compared to other porous materials.

2.2 Design of MOFs

MOF materials possess tunable pore sizes, structure diversity, and other advantages. It is very important to get a full knowledge of how these inorganic parts and organic parts are connected to each other for the design of MOF structures. MOFs can be synthesized by self-assembly of organic ligands and metal ions. At the early stage of MOFs' synthesis, direct assembly of new MOFs from particular metal nodes and organic linkers is the main approach. First row transition metals such as Zn, Cu and Co are well known to be able to coordinate with carboxylate groups under hydro and solvothermal conditions to form crystals.

2.2.1 Organic Ligands as Building Blocks of MOFs

The basic requirement for organic ligands is it can form coordination bonds with a central metal or secondary building units (SBU). The pore volume and surface area of MOFs can be controlled by choosing different organic ligands for a specific application.[27] Until now, benzene-carboxylate groups (scheme 1) are the main source due to their rigidity and consequent tendency to form rigid metal carboxylate clusters. Ligands with this linear orientation mostly generate square planar or cubic MOFs.

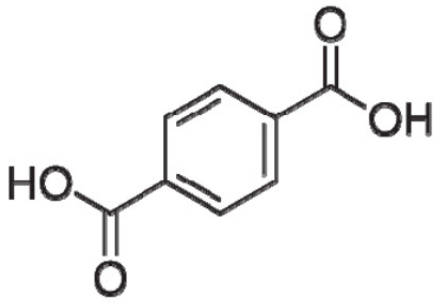

Benzene-1,4-dicarboxylic acid

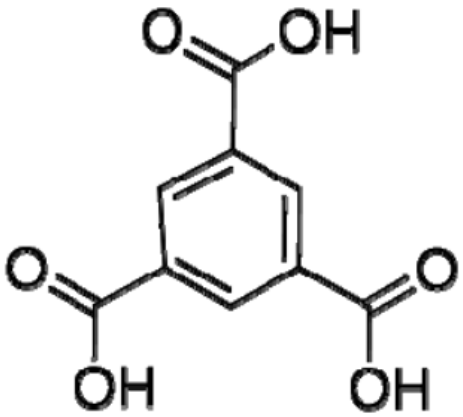

Benzene-1, 3, 5-tricarboxylic acid

Scheme 1. Selected organic ligands with carboxylate groups.

Pyridine and triazole as shown in scheme 2, are also good choices since they contain N atoms which have lone pair electrons that can form coordinate covalent bonds with metal ions.

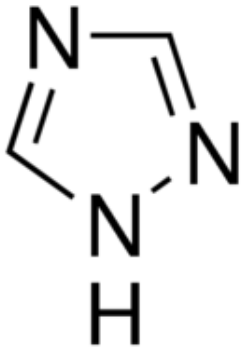

1,2,4-triazole

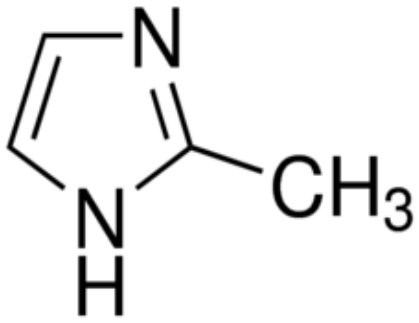

2-methylimidazole

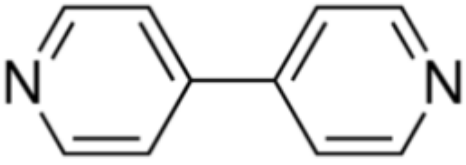

4,4’-bipyridine

Scheme 2. Selected organic ligands with aromatic nitrogen.

2.2.2 Design Methods

Two methods for MOF design have been developed after systematic and comprehensive research on MOFs through many years. One is the templating method and the other involves construction from secondary building units (SBU).[28] The design of the topology of a MOF is more complicated. This relates to the type of linkers as well as SBUs. For example, a tetrahedral linker combined with an 8-connected cubical SBU in a 2:1 ratio could get fluorite (**flu**) topology; however, platinum sulfide (**pts**) topology will result when the same linker is combined with a 4-connected square planar.[29] The SBU forms of MOFs are affected by many variables. For example, larger angle between the carboxylates and the benzene ring induced by other substituents, may lead to larger deformation degree of the SBU.[30]

2.2.3 Post-synthetic Modification

In order to improve the performance of certain aspects of MOF materials, post-synthetic modification has become a focus. Chemical modulation can involve multiple approaches such as doping with metal ions or organic functional groups[31]. In most cases, the pore size and pore shape of a MOF can be controlled through this approach, which can modify the selectivity of a MOF on adsorbed gases and the gas uptake capacities.[32] Cohen and co-workers successfully reacted acetic anhydride with amino groups of IRMOF-3, ($Zn_4O(H_2N\text{-}BDC)_3$), which is an amino-substituted version of IRMOF-1 ($Zn_4O(BDC)_3$). This process is realized by treating IRMOF-3 with dilute acetic anhydride solution in $CDCl_3$ under ambient conditions[31]. Also, it was found that doping with lithium in MOFs could greatly improve H_2 uptake capacity near ambient conditions.[33]

2.3 Synthesis Method

The most widely used method for MOF synthesis is the solvothermal method. This is due to the process being simple and easily controlled. However, there are drawbacks such as time consuming and usually large particle sizes.

2.3.1 Conventional Synthesis

The most popular method of synthesizing MOFs is the solvothermal method. The process of this method is to mix the reactants and solvent together, then seal them in a Teflon reactor, and heat the reactor at a temperature of 100~200^{o}C. The mixture will react under autogenous pressure above the boiling point of the solvent. The reactants dissolve slowly with the increased temperature and react to form nice crystalline products. This method requires less time and the equipment is simple and can be used for certain reactants that are insolvable at or below the room temperature. In addition, most products are perfect crystals, which can then be analyzed by the single crystal XRD technique.[34]

Product formations are greatly determined by the reaction temperature. Usually more condensed structures are observed at higher temperatures[35]. In order to get proper crystals and reaction rates, an increasing reaction temperature is needed for certain MOFs, especially if kinetically more inert ions are used. This method can be used for the syntheses of a wide variety of MOFs which are among the most extensively studied. These include among others: MOF-5, MOF-74, MOF-177, Cu-BTC (HKUST-1) or ZIF-8.[36] This method sometimes termed the direct precipitation reaction, shows that the crystallization of some MOFs take place on a short time-scale[37].

2.3.2 Centrifugal Separation

Recent work has been reported[38] on a rapid room-temperature colloidal chemistry route to produce nanocrystal ZIF-8. The process was to stir the mixture for about two hours after adding a methanolic solution of $Zn(NO_3)_2 \bullet 6H_2O$ into a methanolic solution of 2-methylimidazole. The product was then centrifuged several times and washed with ethanol. After drying the product overnight in an oven, nanocrystals of ZIF-8 were obtained. Monodisperse nano-sized porous materials can have improved its properties for specific application such as gas storage and separation.

2.3.3 Microwave-Induced Thermal Method

Microwave-assisted homogeneous and heterogeneous nucleation of zeolites have already been confirmed to be a useful way to synthesize powders and films of zeolites.[39] Yeonshick[40] developed a novel microwave MOF synthesis method the microwave-induced thermal method, to rapidly synthesize MOF-5. The experiment process was firstly to a prepare precursor solution, then put the substrates which are nanoporous anodized alumina discs coated with various conductive thin films into the container containing the precursor solution. Irradiated with 500W power microwave for 5 to 30 seconds to induce the MOF-5 film growing in the container. The advantages of this method are rapid and the resulting products are nanoporous film with high kinetics.

2.3.4 Ultrasonic Irradiation

Ling-Guang Qiu et al.[41] reported for the first time the synthesis of a fluorescent microporous MOF, $Zn_3(BTC)_2 \bullet 12H_2O$ through a ultrasonic process. Under ambient

temperature and pressure conditions, the reaction of zinc acetate dihydrate and benzen-1,3,5-tricarboxylic acid (H_3BTC) were mixed in a solvent and the mixture was irradiated by ultrasonic for about 5 min. The crystals in nanoscale were obtained with much more higher yield (75.3%) than the crystals synthesized by the hydrothermal method. It was reported the ultrasonic time could increase the yield.

2.4 Applications of MOF Material

2.4.1 Gas Storage

Being porous materials, the application of MOFs on gas is of para,ount importance. Many MOFs have synthesized for CO_2 capture from flue gas.[42] The biggest shortcomings for traditional technologies for gas absorption are that equipment sizes are too large and energy is consumed too high.[43] In contrast to this, MOFs are a low cost, and relatively easily regenerated among other advantages.[44] Additionally, most show promise as storage materials for hydrogen, methane and other clean energy, MOFs have already triggered extensive attention and have achieved encouraging results. For example, MOF-519 exhibits high methane volumetric storage capacity of 279cm^3cm^{-3} at 298K and 80bar has been reported.[13]

2.4.2 Adsorptive Separations

The gas separation process being realized by MOF materials is derived from the differences in adsorption/desorption behavior of components of a mixture.[15] Rational design about the pore sizes and other properties at the molecular level may result in unique interactions with certain guest molecules rather than others and thus achieve

unusual chemicophysical adsorption.[8] For example, homochiral MOFs possess the potential on enantio-separation which is still a challenge.[15]

2.4.3 Biomedical/Drug Deliver

Some MOF materials have high amount of drug loading ability since they possess useful features such as high BET surface area, excellent biocompatibility and functional diversity. Some of them on a nanometer scale might provide an approach to design novel theranostic nanomedical devices. Also some MOFs on the mesoporous scale might possess the ability of loading biological molecules such as anticancer drugs into their pores[45]. Patricia et al. for the first time showed the remarkable capacity of Ibuprofen hosting and delivery by MIL-100 and MIL-101. They also pointed out that the enormous possibilities for the design of new MOFs including their advantages to adapt to the structure of the drugs and their dosage requirements.[46]

2.4.4 Asymmetric Catalysis

Because of their pore structures and large specific surface area, MOFs can be functionalized using metal ions and ligands to produce catalytic sites. In the last few decades, researchers have recognized that MOFs could be used in asymmetric catalysts after incorporation of a chiral ligand or proper chiral catalytic units or open metal sites or inside pores.[47] POST-1 is the first example of MOFs which exhibited catalytic features for an asymmetric chemical reaction as reported by Kim et al.[48] The advantages of MOFs as asymmetric catalyst are they avoid the tedious separation process as required in a general synthesis method which yield for racemic mixtures and they don't require large

amounts of chiral agents as in the traditional stoichiometric synthetic method. Furthermore, they could increase the yields of the pure enantiomers.[47]

2.4.5 Luminescent Materials

Luminescent materials have a broad application in lighting, organic pigments, drug tracer and many other area.[49] Traditional luminescent materials include inorganic and organic luminescent materials. MOF materials are very promising as a multifunctional luminescent material because both the organic and the inorganic part can produce luminescence. Additionally, ligand to metal charge transfer (LMCT) and metal to ligand charge transfer (MLCT) may also result as a luminescence property of certain MOF materials.[45] Yuexin Guo[14b] synthesized TABD-MOF-1, -2, -3 which were constructed from Mg^{2+}, Ni^{2+}, and Co^{2+}, respectively with deprotonated 4,4'-(Z,Z)-1,4-diphenylbuta-1,3-diene-1,4-diyl as sensors. Their luminescent properties were modified by changing metal ions. When using specific metal ions, the luminescent feature of this sensor could be "turned off" and only "turned on" when it was exposed to a five-membered heterocyclic ring explosives. The "fluorescence switch" may be triggered quickly and was very sensitive.

CHAPTER III

Research Methods and Instruments

3.1 Materials and Synthesis Method

3.1.1 Chemicals

Table 3-1 is a list of chemicals used in this research project.

Table 3.1 all the chemicals used in this project

Name of the chemical	Formula	Company Name	Grade
1,2,4-triazole	$C_2H_3N_3$	Aldrich	98%
Copper(II) sulfate pentahydrate	$CuSO_4 \cdot 5H_2O$	Aldrich	Lab Grade crystals
2-methylimidazole	$C_4H_6N_2$	Alfa Aesar	97%
Zinc Nitrate hexahydrate	$Zn(NO_3)_2 \cdot 6H_2O$	Alfa Aesar	99%
Benzene 1,3,5-tricarboxylic acid	$C_6H_3(CO_2H)_3$	Alfa Aesar	98%
Copper(II) nitrate trihydrate	$Cu(NO_3)_2 \cdot 3H_2O$	Fischer scientific	Lab Grade crystals
2,5-dibromoterepthalic acid	$C_8H_4Br_2O_4$	Accela	97%
Cobalt(II) nitrate hexahydrate	$Co(NO_3)_2 \cdot 6H_2O$	Mallinckrodt, INC	
Triethylamine	$C_6H_{15}N$	Alfa Aesar	99%
N,N'-dimethylformamide	C_3H_7NO	Alfa Aesar	99.8+%
Methanol	CH_3OH	Alfa Aesar	Lab Grade
Ethanol	C_2H_5OH	Alfa Aesar	Lab Grade
Nitrogen gas	N_2	Air Gas	Compressed

3.1.2 Hydro/Solvothermal Synthesis

The main steps of hydro/solvothermal synthesis are to mix reactants into a solvent and heat to a certain temperature (several hundred degrees Celsius) in the steel pressure vessel (autoclave) Crystals grow under autogenous pressure. The autoclaves must be made by thick steel material which could stand a high-pressure and high-temperature environment for a long synthesis time. Figure 3.1 shows an autoclave used in this thesis research.

Figure 3.1 Autoclave used in the synthesis

3.2 Instruments

3.2.1 Single Crystal X-Ray Diffraction

Crystal lattice structures can diffract X-ray, and the diffraction information corresponds with specific crystal structure information. Therefore, the crystal information

including crystal symmetry, unit cell dimensions, details of site-ordering, atomic positions and space group can be identified by studying its diffraction ray. The X-ray single crystal diffraction equipment is designed based on this theory. It mainly includes the emitter, sample stage, detector and signal conversion. The emitter is a cathode ray tube that could generate X-ray. Signals will be detected by the detector. The single crystal used for the single crystal X-ray diffraction should have a regular shape without cracks and blemishes; color and transparency should be consistent. The size of the crystal between 0.3 mm to 0.7 mm is reasonable.

The instrument used for single crystal X-ray Diffraction in my project is Bruker Quazar diffractometer. The data was processed with the SAINT software[50] and corrected for absorption with SAD-ABS[51].

Figure 3.2. Bruker Quazar Single Crystal X-ray Diffractometer.

3.2.2 Powder X-Ray Diffraction

Once the crystal structure of a new compound is determined by the single X-ray diffraction, powder X-ray diffraction could be used to test if the synthesized sample possessed the same crystal structure with the single crystal or not. Powder X-ray diffraction is a rapid analytical and non-destructive analytical technique used for phase identification. In addition, powder X-ray not only can be used for crystal quantitative analysis, but also could determine the lattice parameter, grain size and miller index precisely.

The X-ray usually emitted by “Cu” atom or “Mo” atom and the sample should be finely grounded before testing to diminish its preferred orientation.

Figure 3.3. ARL Thermo Powder X-Ray Diffractometer.

The instrument used for Powder X-Ray Diffraction in my project is the ARL Thermo X-ray Diffractometer with Cu-Kα radiation. The sample was swept from 2θ=3º

to 60º with a speed of 1.2º/minute. The X-ray generator was set to 20 kV and 20 mA. The picture of the ARL Thermo X-ray Diffractometer is shown in Figure 3.3

3.2.3 Carbon Hydrogen and Nitrogen Analyzer

Most elemental analyses such as C, H, N and S are based on redox reaction. Samples are finely grounded, wrapped by a tin foil and delivered to the combustion tube by an autosampler. A small amount of pure oxygen is used to aid combustion of organic or inorganic samples. After combustion, samples undergo further catalytic redox processes to convert C, H, and N to a variety of detectable gases.

The instrument used in my project for C, H, N and other element determination is Leco True-Spec CHN Determinator. The carrier gas is helium in 99.99% purity and the pressure is 35psi±10%. The purity of the oxygen is 99.99% and the pressure is 35psi± 10%. The furnace used for combustion can be heated up to as high as 1050℃.

Figure 3.4. Leco True-Spec CHN Analyzer.

3.2.4 Thermogravimetric Analysis

The thermogravimetric analysis is a technique used for measuring the quality change of a material with temperature changes. It is understood that the measured mass of a sample will change when it undergoes sublimation, vaporization, decomposition or loss of crystalliferous water. If any of these processes take place, then the thermogravimetric curve will make a sharp decline. Through thermogravimetric analysis, analysts can get information such as at what temperature the mass of samples can change, or how much matter was lost.

Instrument Hi-Res TGA 2950 thermal gravometric analyzer was used to test the thermal stability of samples. The flow nitrogen atmosphere in the rate of 15ml/min. The temperature ramp rate is 10 ℃/min from 23℃ to 700℃. Figure 3.5 is the picture of the equipment.

Figure 3.5. Hi-Res TGA 2950 thermal gravimetric analyzer.

3.2.5 Infrared Spectroscopy

Infrared spectroscopy is a useful analytical technique for structure analysis and functional group identification of materials. The basic principle of infrared spectroscopy is vibrations of molecules in a sample can absorb infrared radiations with specific wavelengths. Every material possesses unique infrared spectrum decided by its structures and symmetry. Thus, infrared spectroscopy could be used for qualitative analysis.

The infrared spectra were recorded from 400 to 4000 cm^{-1} on a Perkin Elmer Spectrum One FTIR spectrometer using KBr pellets. The background scan was collected with KBr pellets.

Figure 3.6. Perkin Elmer Spectrum One FTIR spectrometer.

3.2.6 Scanning Electron Microscope（SEM）

The principle of SEM is when a sample is scanned using a very thin high-energy electron beam, the excited region can produce secondary electrons, Auger electrons,

characteristic X-ray and other microscopic particles. Therein, the secondary electrons came from 5-10 nm depth of the surface and they are very sensitive to the state of the sample surface and can effectively show the sample morphology. The SEM instrument is composed of an electron optical system, a signal collection and display system, a vacuum system and a power system. For purpose of this research, all the SEM tests were realized by JEOL 5400LV scanning electron microscope (SEM) at an accelerating voltage of 20 kV after gold-palladium mix deposition. Figure 3.7 is the picture of the equipment.

Figure 3.7. JEOL 5400LV scanning electron microscope (SEM).

3.2.7 Transmission Electron Microscope (TEM)

TEM is a microscope in which samples are irradiated with an accelerated electron beam. The electrons will change directions of movements when colliding with atoms of the sample, thereby producing solid angle scattering. The size of the scattering angle of the sample relates to density and thickness of the sample, and can form images with different light and shade. The main parts of the TEM are the electron gun, collecting

mirror, sample room, and transmission mirror. All the TEM images exhibited in this research project were realized by JEM-1400 Plus Electron Microscope. Figure 3.8 is the picture of the instrument.

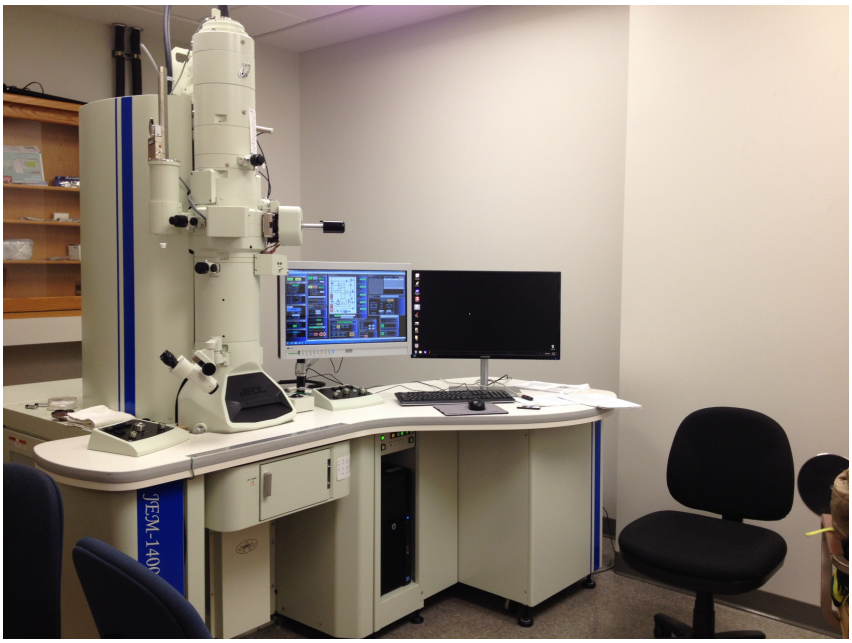

Figure 3.8. JEM-1400 Plus Electron Microscope.

3.2.8 Mercury Absorption Test

Mercury absorption test was conducted on a fixed bed bench scale sorbent screen facility at the Institute for Combustion Science & Environmental Technology of WKU. Tests were carried out using a simulated gas similar totypical flue gas constituents from firing the Powder River Basin coal. The gas stream passed through a temperature-controlled fixed-bed column containing ~100 mg of sorbents at 150 °C

CHAPTER IV

Synthesis, characterization and mercury absorption test of known MOFs: $[Cu_3(trz)_3(OH)_3(H_2O)_4]\cdot 4.5\ H_2O$, $Zn(MeIM)_2$ and $Cu_3(BTC)_2(H_2O)_3$

4.1 Introduction

The first part of my project was to investigate the mercury absorption properties of selected known porous MOFs using simulated flue gases. $[Cu_3(trz)_3(OH)_3(H_2O)_4]\cdot 4.5\ H_2O$ (**1**), $Zn(MeIM)_2$ (**2**) and $Cu_3(BTC)_2(H_2O)_3$ (**3**) were selected based on their excellent thermal stabilities and larger pore sizes. The solvent accessible void of **1** is 41.4% of the unit cell volume with pores of 17×13×13Å. The framework of **1** can be stable as high as 300°C,.[52] **2** has extremely high BET surface area and Langmuir surface area, both of which are more than $1500 m^2/g$.[53] Its thermal stability can be up to 500°C. **3** possesses the BET surface area of $692.2 m^2/g$ and Langmuir surface area of $917.6 m^2/g$[54]. Its framework structure can keep intact as high as 240°C. In addition, the framework of **3** has open metal sites after coordinated water molecules are removed. Studies have shown that gases such as H_2 and CO_2 can be absorbed on the copper open metal sites,[55] it is expected that these metal site can enhance the absorption of mercury as well.

These three materials were prepared using the methods descripted in literature and their structures and stabilities were analyzed by PXRD, and TGA and mercury absorption was examined on a fixed bed bench scale sorbent screen facility.

4.2 Synthesis

*4.2.1 Synthesis of $[Cu_3(trz)_3(OH)_3(H_2O)_4]\cdot 4.5\ H_2O$ (**1**)*

1 was synthesized according to the following experiment procedure[52] through the hydrothermal reaction. Copper sulfate pentahydrate 0.163 g ($CuSO_4 \cdot 5H_2O$, 0.628 mmol), 1,2,4-triazole 0.048 g (Htrz, 0.694 mmol), and DI water 5.00ml (556 mmol) were mixed together into a 23 mL PTF cup. After stirred briefly, the cup was sealed and heated at 200°C for 48 h. After cooled to room temperature, products were filtered, washed with deionized water, and dried in air over night. Blue octahedral crystals of $[Cu^{II}_3(trz)_3(OH)_3(H_2O)_4]\cdot 4.5\ H_2O$ were obtained.

*4.2.2 Synthesis of $Zn(MeIM)_2$ (**2**)*

2 was synthesized according to Janosch Cravillon et al.[36] First zinc nitrate hexahydrate 0.587 g (0.00197 mol), and 2-methylimidazole (MeIM) 1.298g (0.0158 mol) were dissolved into 40 mL of methanol separately and stirred briefly. Then the MeIM solution was poured into the $Zn(NO_3)_2\cdot 6H_2O$ solution. The mixture was stirred at room temperature for 2 h resulting in a milky colloidal gel. Then, the milky colloidal was centrifuged for 15 min and washed with ethanol. The centrifugation was repeated three times. After centrifugation, the product was dried at 60℃ for 12h. Finally, white crystalline products of $Zn(MeIM)_2$ were obtained

*4.2.3 Synthesis of $Cu_3(BTC)_2(H_2O)_3$ (**3**)*

3 was synthesized according to Donald J. Darensbourg et al.[56] $Cu(NO_3)_2 \cdot 3H_2O$ (1.419 g, 0.00589 mol) was added into 6.0 mL DI water and stirred till it was dissolved. Meanwhile, BTC (1,3,5-benetricarboxylate acid 0.619 g 0.00279 mol) was dissolved in 6.0 mL ethanol. These two solutions were mixed and transferred a 23mL PTF cup. The cup was sealed, placed into an oven and heated at 110℃ for 18h. After the oven was cooled to room temperature, products of dark-green crystals were filtered, washed with deionized water, and dried in air over night.

4.3 Results and Discussion of $[Cu_3(trz)_3(OH)_3(H_2O)_4]\cdot 4.5\ H_2O$ (1)

4.3.1 The Structure Description of ***1***

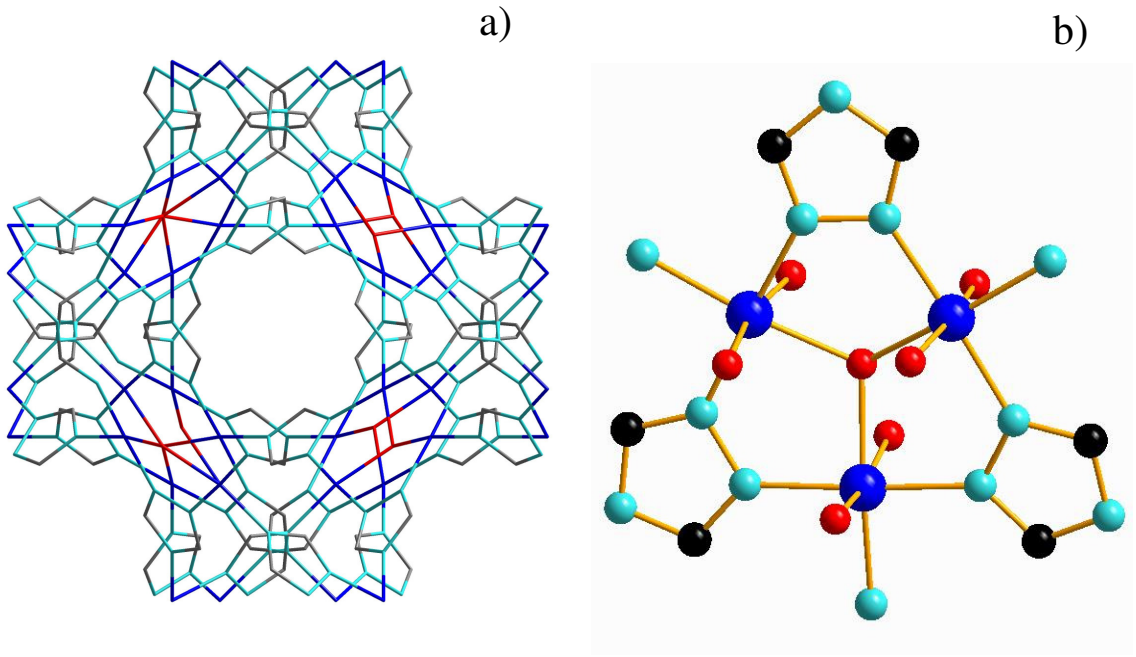

Figure 4.1. (a) A wire representation of the 3D structure of $[Cu_3(trz)_3(OH)_3(H_2O)_4]\cdot 4.5\ H_2O$ (**1**), (b) Coordination environment of copper. Black: C Blue: Cu Red: O Cyan: N.

Figure 4.1a shows the 3D open framework structure of compound **1**. Each Cu ion connects with three N atoms from three 1,2,4-triazole molecules, one μ_3-OH^- group, two terminal water molecules, or one water and on terminal OH^- group. In total, there were six coordinating ligands for each Cu, forming a distorted octahedron configuration. The Cu_3N_6 triangular ring (Figure 4.1b) can be considered as a cluster. Each cluster links to six same clusters in equatorial and axial positions, forming a three-dimensional structure with three-dimension channels.

*4.3.2 Thermal Stabilities of $[Cu_3(trz)_3(OH)_3(H_2O)_4]\cdot 4.5\ H_2O$ (**1**)*

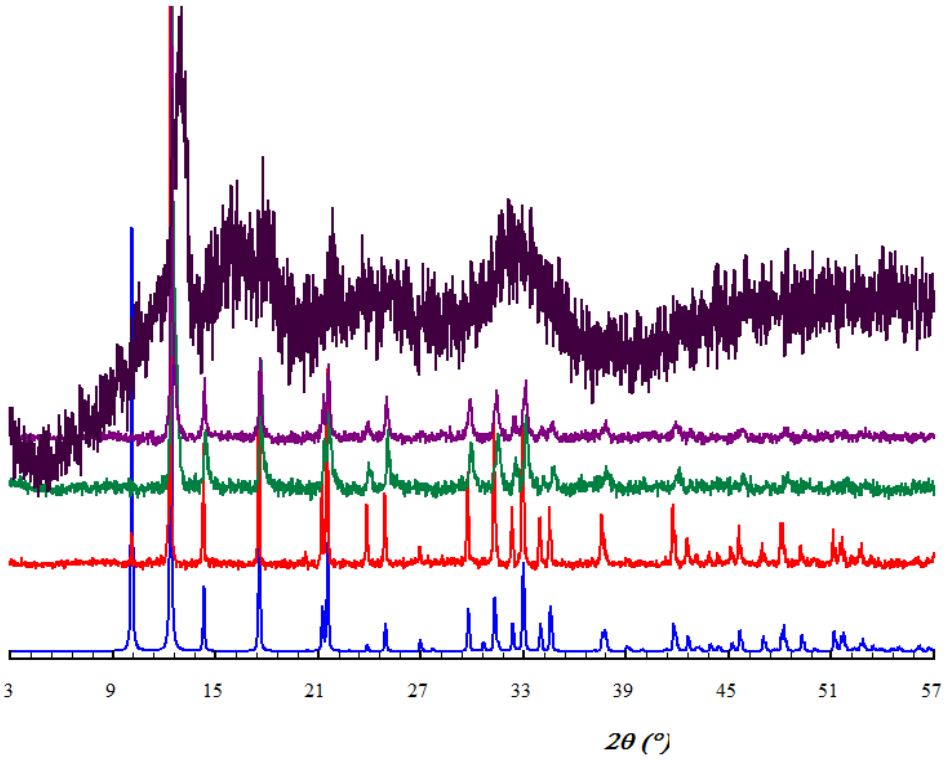

Figure 4.2. Thermal stabilities of $[Cu_3(trz)_3(OH)_3(H_2O)_4]\cdot 4.5H_2O$ (**1**). Blue: simulated from SXRD. Red: experimental; Green: heated at 150°C for 12h; purple: heated at 180°C for 12h; black: heated at 210°C for 12h.

Figure 4.2 is PXRD patterns for samples of **1** after heated at different temperatures for 12h. PXRD patterns of samples heated at 150 °C and 180 °C show no differences from those of the unheated samples or the simulated PRXD patterns. This suggested that the framework of 1 stable up to 180 °C. After heated at 210°C for 12h, compound **1** changed to amorphous, as can be seen from the PXRD pattern in Figure 4.2.

*4.3.3 Thermal-gravimetric Analysis of [$Cu_3(trz)_3(OH)_3(H_2O)_4$]·4.5 H_2O (**1**)*

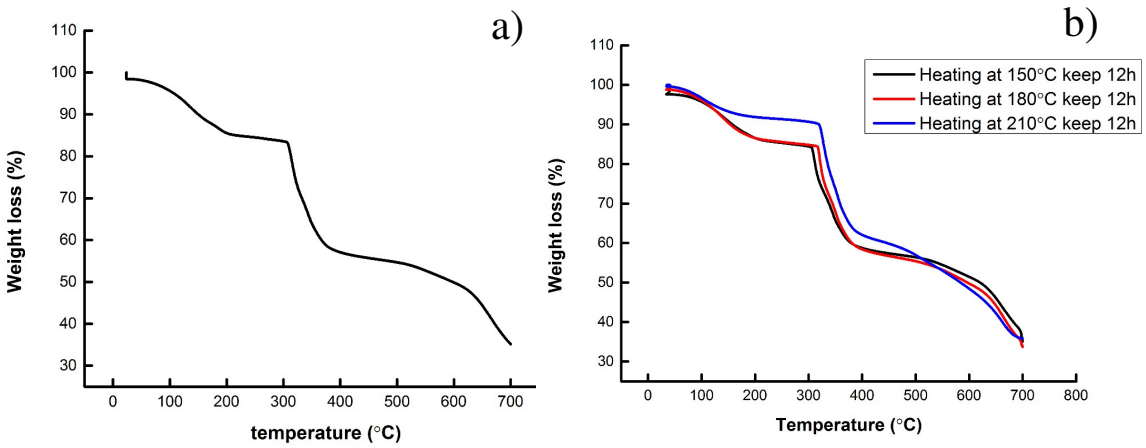

Figure 4.3. (a) TGA plot of [$Cu_3(trz)_3(OH)_3(H_2O)_4$]·4.5$H_2O$ (**1**) before heating, (b) TGA plots of 1 after heating at 150°C, 180 °C and 210 °C kept for 12h.

As shown in the TGA plot in Figure 4.3, a 13.43% weight loss between room temperature and 186°C is observed for compound **1**. This is corresponding to the removal of 4.5 crystallization water molecules per formula unit. The PXRD pattern of **1** after heated at 180°C for 12h has shown the framework structure of is stable after the removal of water at this temperature. The removal of coordination water and the decomposition of the organic ligand are observed in two steps: from 300°C to 360°C, and from 600°C to 700℃.

In order to study the temperature at which the crystalline water is removed, samples of compound **1** were heated in an oven at different temperatures followed by TGA analysis of the heated samples. Figure 4.3(b) shows the TGA plots of samples of **1** heated at a 150, 180, 210°C. Among them, the blue line refers to the sample after heated at 150°C for 12h, the orange line represents the sample after heated at 180°C for 12h and the grey line is the sample heated at 210°C for 12h. The TGA plots of the samples heated at 150 °C and 180 °C show no significant difference. However, the TGA plot of the sample after heated at 210°C shows a significant difference in the temperature of 120°C-500°C from those of heated at 150 °C and 180 °C. This suggested the sample heated at 210 °C before TGA had partially lost its coordination water, therefore the TGA weight loss of the sample heated at 210°C is less than those of the samples heated at 150°C and at 180°C.

*4.3.4 SEM Measurement of $[Cu_3(trz)_3(OH)_3(H_2O)_4]\cdot 4.5\ H_2O$ (**1**)*

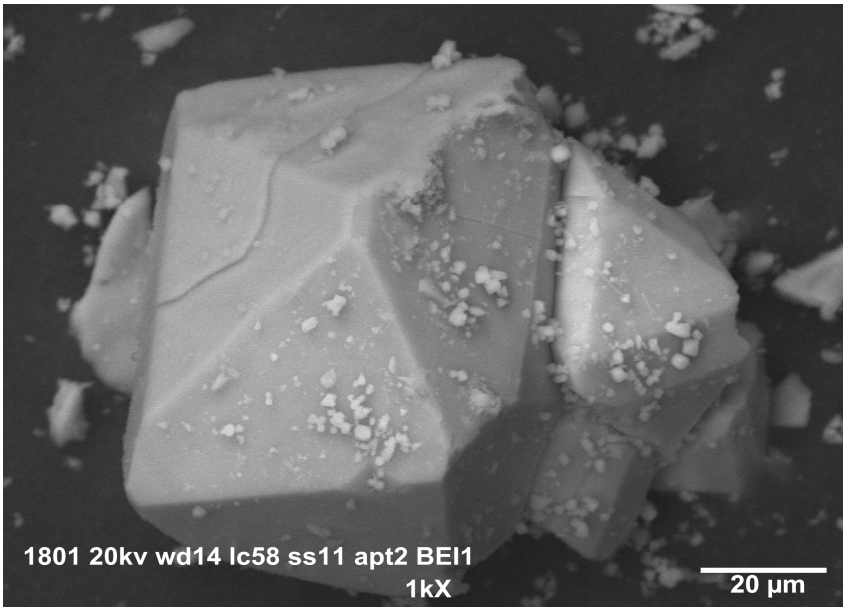

Figure 4.4. SEM image of $[Cu_3(trz)_3(OH)_3(H_2O)_4]\cdot 4.5H_2O$.

Figure 4.4 shows the SEM image of **1**. It can be seen that the crystal is octahedral, and the edge length is about 40 μm. Particle size distribution is important for the absorption ability of sorbents.[57] Usually, smaller-sized particles lead to higher surface area and thus stronger adsorption capacity. It also can increase the overall adsorption kinetics.

*4.3.5 Mercury Absorption Test of [$Cu_3(trz)_3(OH)_3(H_2O)_4$]·4.5 H_2O (**1**)*

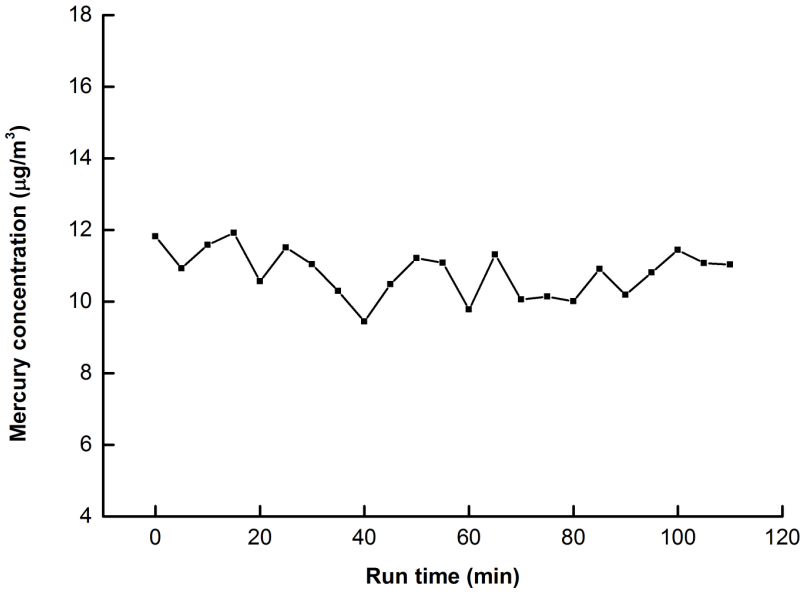

Figure 4.5. Mercury absorption measurement of [$Cu_3(trz)_3(OH)_3(H_2O)_4$]·4.5$H_2O$ (**1**).

We tested the mercury absorption ability of the framework of **1** on simulated flue gas using a fix bed furnace. The sample for mercury absorption experiments was prepared by heating **1** in an oven at 150℃ for 12h to remove the crystalline water. Figure 4.5 shows the mercury absorption plot. The plot indicated that the mercury concentration

of the simulated flue gas passing through the sample did not change significantly, suggesting that the sample of compound **1** did not absorb significant amount of mercury. There are a number of reasons that the sample we tested for mercury absorption did show expected activity. First, it is possible only a small portion of the water in the pores of **1** was removed at 150℃.[8] Second, the sample may have low selectivity on mercury over other gas molecules such CO_2 or N_2. Third, large pore sizes do not necessary lead to higher absorption capacity. The materials should have appropriate pore sizes for the kinetic diameters of the guest molecules. The size of the pores often plays a critical role in the absorption process.[58]

This results suggest that it is necessary to incorporate functional group such as S[59] and Cl in the pores of the framework materials to enhance their mercury absorption. As previously mentioned, mercury prefers to be absorbed in divalent form such as HgS[57] or $HgCl_2$. Most researchers proved that the mercury absorption process was not only a physical absorption process but also a chemical adsorption process.[60] Thus, incorporation of functional groups may increase chemical absorption.

4.4 Results and discussion of $Zn(MeIM)_2$ (2)

*4.4.1 The Structure of $Zn(MeIM)_2$ (**2**)*

a)

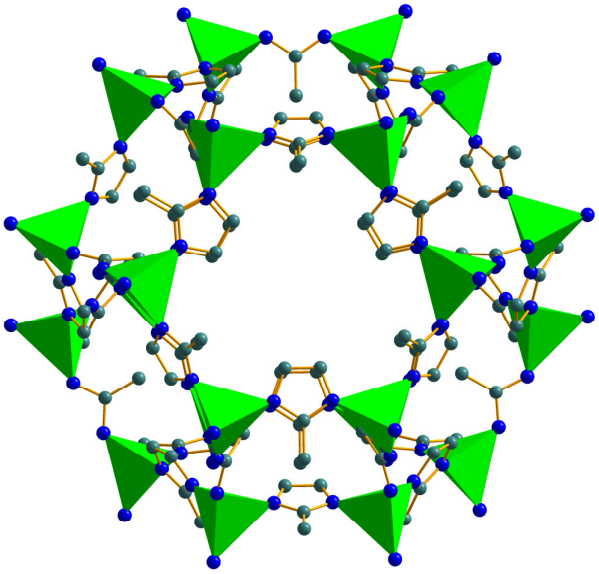

b)

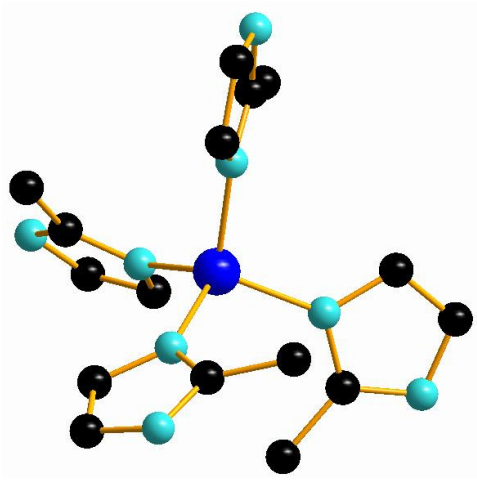

Figure 4.6. (a) Three dimensional structure of $Zn(MeIM)_2$ (**2**) (b) Coordination environment of Zinc. Blue: Zn; Black: C; Cyan: N.

As shown in Figure 4.6, the Zn ion is four-coordinated with nitrogen atoms from four MeIM molecules. These four nitrogen atoms form a tetrahedron. There are two kinds of rings in this structure: one is a 12-membered ring composed by 6 units of Zn-N tetrahedral and 6 units of MeIM, another is an 8-membered ring composed by 4 units of Zn-N tetrahedral and 4 units of MeIM. 8 units of the 12-membered ring and 8 units of the 8-membered ring compose a cage, extended in this structure periodically, resulting in three dimensional channels, and resulting in extremely high BET and Langmuir surface area of more than 1500 m^2/g.[38] The angle of metal-IM-metal is close to 145°, that is similar to the Si–O–Si angle of zeolite structure (Si–O–Si angle is 144°).[61]

*4.4.2 Thermal Stabilities of Zn(MeIM)$_2$ (**2**)*

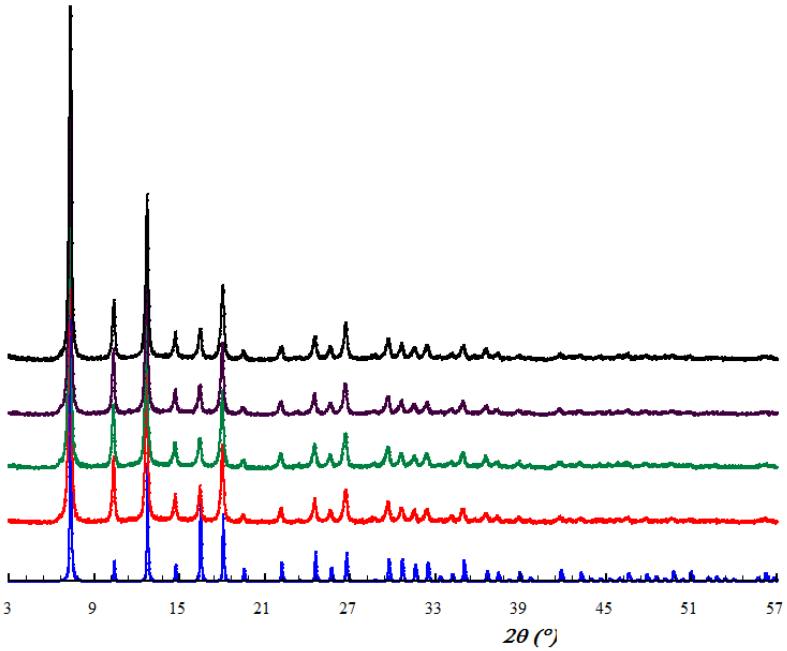

Figure 4.7. Thermal stabilities of Zn(MeIM)$_2$ (**2**). Blue: simulated from SXRD. Red experimental; Green: heated at 150°C for 12h; purple: heated at 180°C for 12h; black: heated at 210°C for 12h.

PXRD was used to study the stabilities of the framework of **1** after heated at 150, 180 °C and 210 °C for 12h. As shown in Figure 4.7, the PXRD patterns remain the same after **1** was heated at 210 °C for 12h. Moreover, its structure is stable even boiled in benzene, methanol, water, and aqueous sodium hydroxide for 1-7 days.[62] The PXRD patterns collected at designated intervals showed that the samples keep their three-dimensional structures intact. Its high resistance to water and temperature could be explained by two aspects. First, the hydrophobic $-CH_3$ (methyl) group could prevent water molecules from attacking the Zn-N tetrahedron units. Second, the bond between IM and Zn/Co is among the most stable of N-donor ligands.[62-63]

*4.4.3. Thermogravimetric Analysis of $Zn(MeIM)_2$ (**2**)*

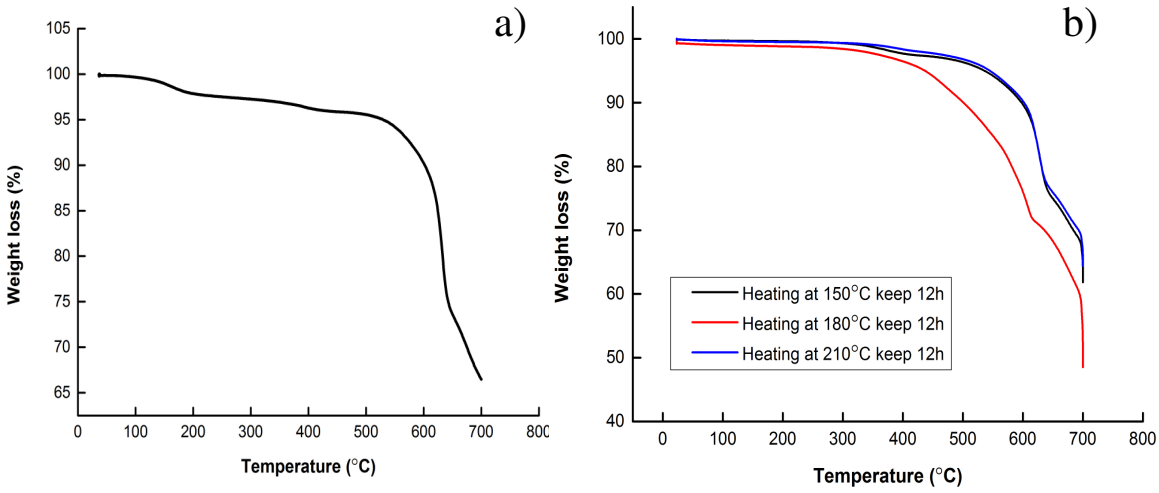

Figure 4.8. TGA plot of $Zn(MeIM)_2$ (**2**) before heating, (b) TGA plots of **2** after heating at 150°C, 180°C and 210 °C kept for 12h.

The thermal stability of compound **2** was investigated by thermal gravimetric analysis. As shown in figure 4.8a, the TGA curve exhibits a gradual mass loss more than 33 % from 30 °C to ca. 700 °C, which is attributed to the removal of part of guest

molecules such as methanol and maybe some residual ethanol from the cavities. Although TGA plot of compound **2** does not show major mass lost below 500°C, optical inspection of the sample powder showed that its color has changed from white to light yellow after heated at 210°C for 12h. This suggests some structural changes such as the coordination number change of metal ions have happened. The sample started to decompose at around 550°C. TGA plots of the samples after heated at different temperatures indicate that the solvent or guest molecules can be removed by heating.

*4.4.4 TEM Image of $Zn(MeIM)_2$ (**2**)*

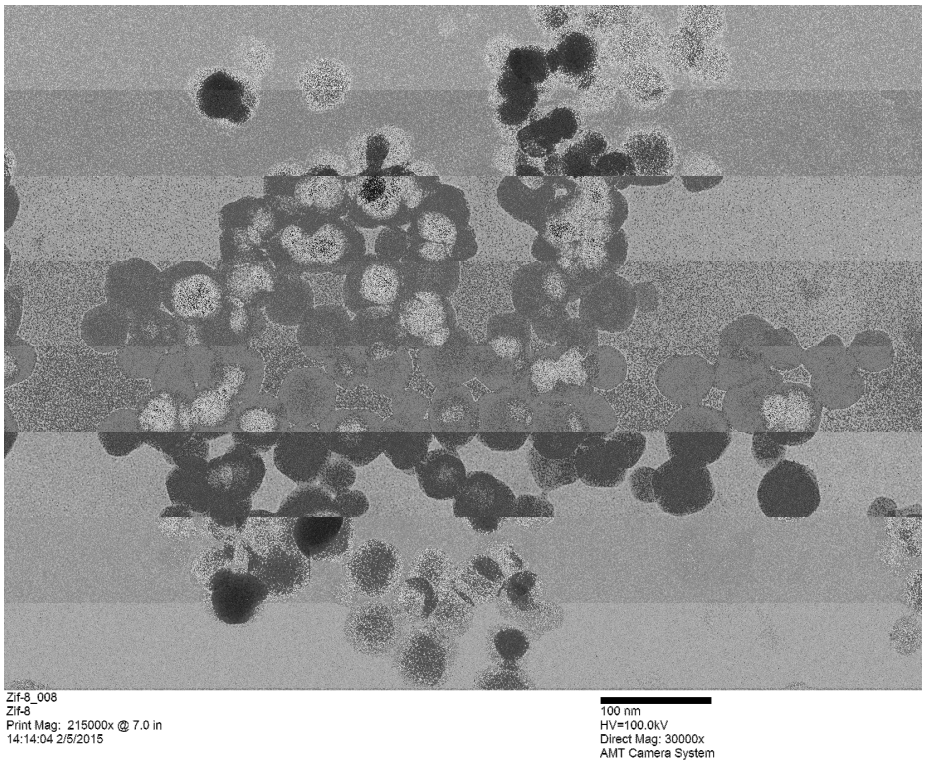

Figure 4.9. TEM image of $Zn(MeIM)_2$ (**2**).

The TEM image of **2** as nanoparticles is shown in Figure 4.9. The uniform particles are between 30 nm and 50 nm in diameter. Most of the particles are spherical, corresponding to its 3D structure analysis.[64]

*4.4.5 Mercury Absorption Test of Zn(MeIM)$_2$ (**2**)*

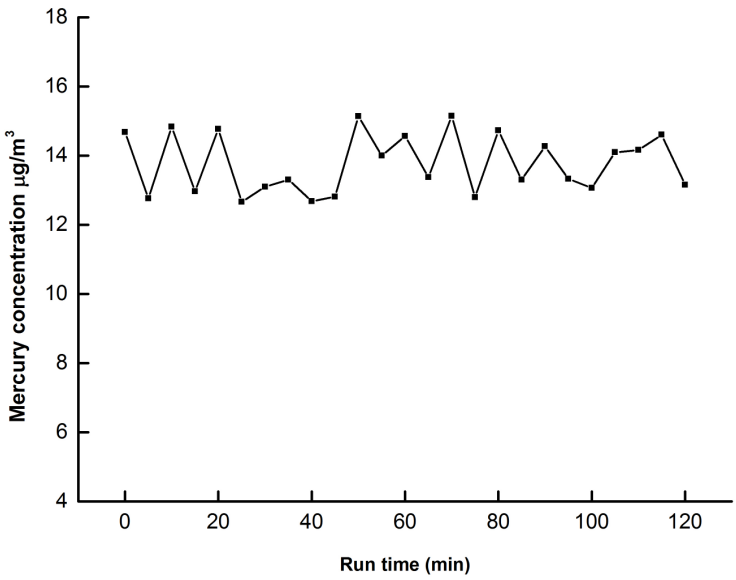

Figure 4.10. Mercury absorption measurement of Zn(MeIM)$_2$ (**2**).

The sample of **2** for mercury absorption test was prepared by heating the sample at 180 °C for 12 h to remove any solvent or gust molecules in the framework of **2**. Figure 4.10 shows the mercury absorption test result of **2**. Simulated flue gas with the mercury concentration of 14.0μg/m^3 was allowed to pass through a fixed-bed furnace loaded with a sample of **2** for 70 mins. No significant changes of mercury concentration in the simulated flue gas were observed after the flue gas passed through the sample. This result

suggests the sample of **2** did not show expected absorption ability even though it possesses high surface area (BET surface 1650m^2/g)[36].

4.5 Results and Discussion of $Cu_3(BTC)_2(H_2O)_3$ (3)

*4.5.1 Structure of $Cu_3(BTC)_2(H_2O)_3$ (**3**)*

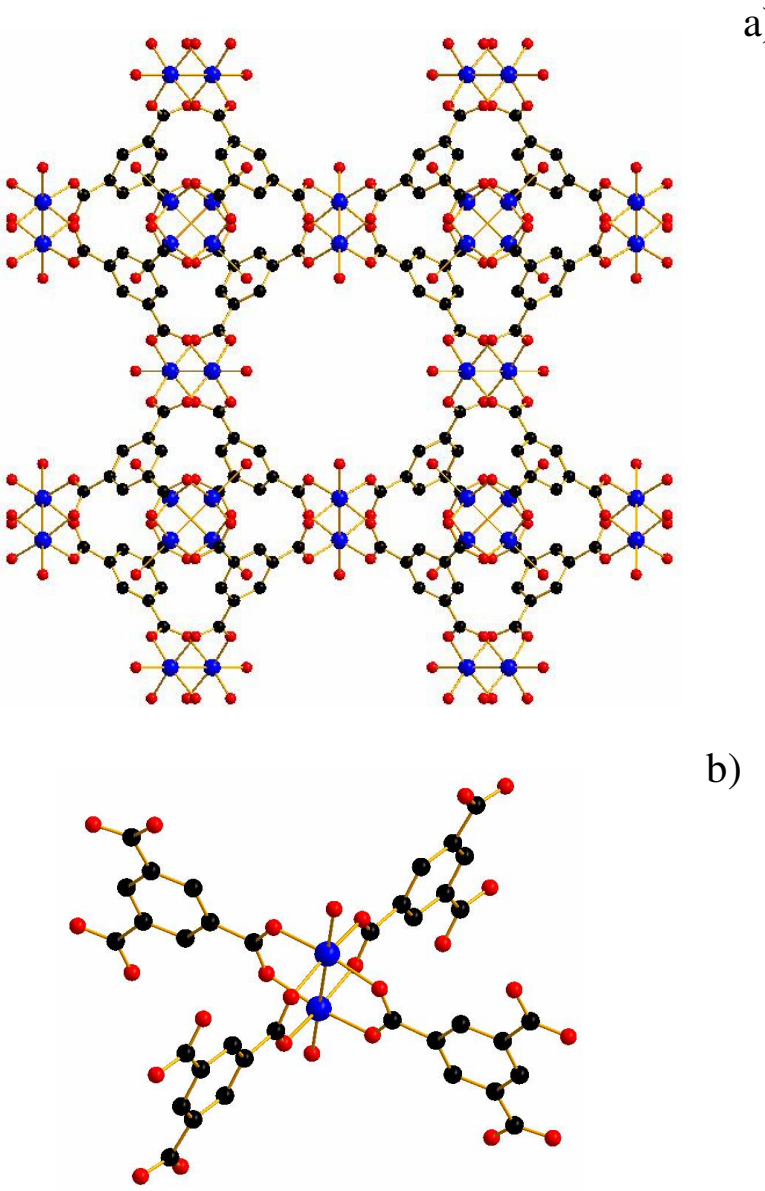

Figure 4.11. (a). Three dimension structure of $Cu_3(BTC)_2(H_2O)_3$ (**3**). (b). Coordination environment of copper Black: C; Red: O; Blue: Cu.

The framework of **3** is a 3D coordination structure with 3D channels (as shown in Figure 4.11). The secondary building unit of **3** has a tetracarboxylate paddlewheel configuration containing two metal ions bonded to four benzene tricarboxylate (BTC) linkers as shown in figure 4.11b. They bonded together through BTC ligands, and extended to three dimensions to form a 3D channel structure which is composed of large central cavities (diameter 9.0 Å) surrounded by small windows (diameter 3.5 Å).[65] The water ligands weakly bonded to Cu atoms. These coordinated waters can be removed by heating and leave the framework of 3 with open metal sites on Cu ions..

4.5.2 Thermal Stabilities of $Cu_3(BTC)_2(H_2O)_3$ (3)

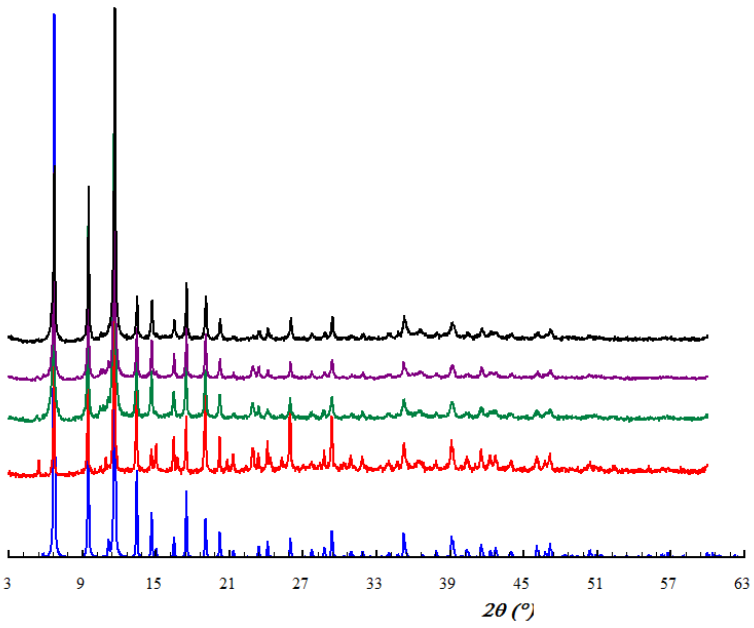

Figure 4.12. Thermal stabilities of compound $Cu_3(BTC)_2(H_2O)_3$ (**2**). Blue: simulated from SXRD. Red experimental; Green: heated at 150°C for 12h; purple: heated at 180°C for 12h; black: heated at 210°C for 12h.

As shown in Figure 4.12, thermal stabilities of **3** were studied by heating sample of **3** at different temperatures in an oven for 12 h. The heated samples were examined with PXRD for their crystal structures. Simulated XRD patterns from single crystal structure, [66] and experimental PXRD for sample without preheating are also include in Figure 4.12. The PXRD plots in Figure 4.12 show on changes in the experimental temperature range in comparison with the simulated PXRD patterns, suggesting the stability of the framework of **3** at 210 °C.[67]

*4.5.3 Thermogravimetric Analysis of $Cu_3(BTC)_2(H_2O)_3$ (**3**)*

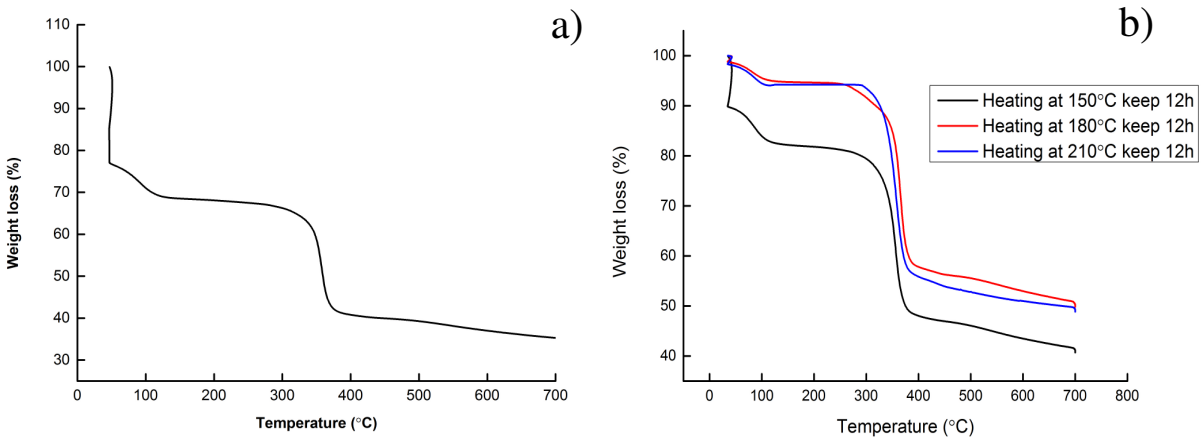

Figure 4.13. (a) TGA plot of $Cu_3(BTC)_2(H_2O)_3$ (**2**) before heating. (b) TGA plots of **3** after heating at 150°C, 180 °C and 210 °C kept for 12h.

Figure 4.13a shows the TGA plot of **3** before it was heated in an oven. The weight loss before 140 °C can be attributed to crystalline water and coordinated water molecules. The weight loss in the range 345°C -385°C can be attributed to the decomposition of the organic ligand.

TG analysis was performed as well on samples of **3** that had been heated at different temperatures in an oven. As shown in Figure 4.13, after the sample of **3** heated at 180 °C or 210 °C most of the water molecules are removed. Our PXRD results showed that **3** is stable up to 210 °C. These results suggested that water can be removed from the framework structure of **3**, but the framework did not collapse.

*4.5.4 SEM Measurement of $Cu_3(BTC)_2(H_2O)_3$ (**3**)*

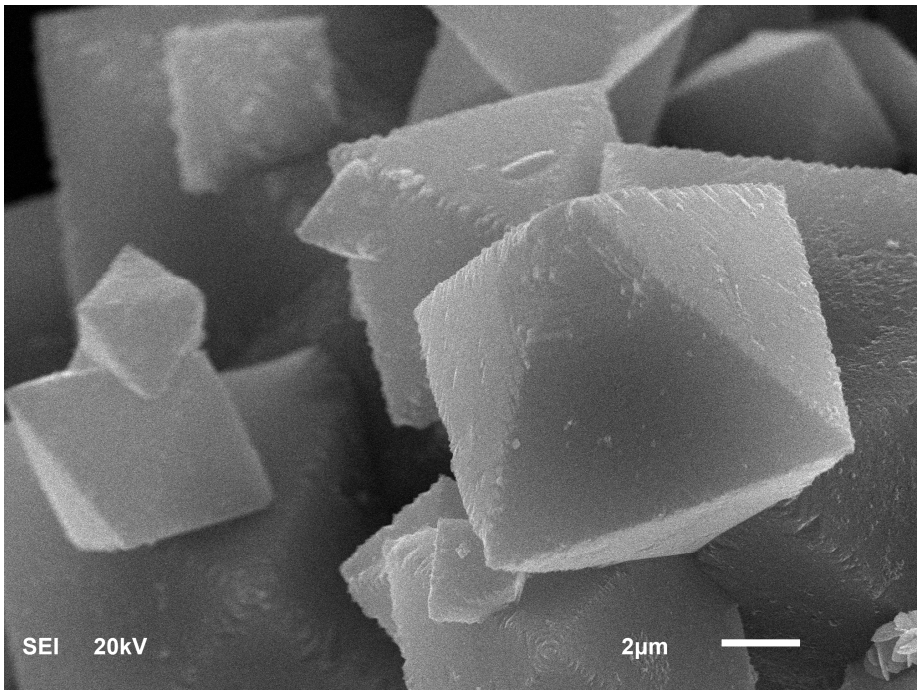

Figure 4.14. SEM image of $Cu_3(BTC)_2(H_2O)_3$ (**2**).

As shown in Figure 4.14, the crystals of all samples of **3** were octahedral. The particle sizes are similar and around 4-10 micrometers.

*4.5.5 Mercury Absorption Test of $Cu_3(BTC)_2(H_2O)_3$ (**3**)*

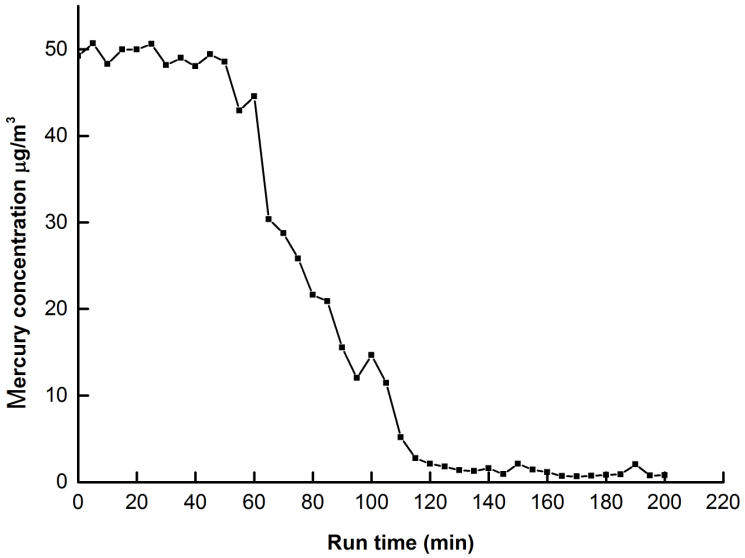

Figure 4.15. Mercury absorption pattern of $Cu_3(BTC)_2(H_2O)_3$ (**2**).

Samples of **3** used for mercury test were heated at 180 °C for 12h beforehand to remove water in the framework. As shown in Figure 4.15, the mercury concentration in simulated flue gas has decreased significantly (over 90%) after the flue gas passed through the sample in a fix-bad furnace. This indicated that **3** has excellent mercury absorption ability under the experimental condition.

For all the three selected MOFs, they all are stable at the experimental condition and all have excellent surface areas. However, only **3** shows excellent mercury absorption ability. One possible explanation is that the framework of **3** has open metal sites which is highly effective for gas absorption.[42] Generally speaking, smaller pore sizes would produce stronger attraction forces acting on the adsorbent molecules due to the overlapping potentials from the surrounding walls.[42] The framework structure of **3** has

large cavities and relatively small openings. This could help enhance its ability on mercury absorption as well.

4.6 Conclusions

Three known porous MOF materials were synthesized using the hydrothermal method. The porous frameworks of these materials are stable after the guest molecules/solvents were removed by heating in air. Among these three framework materials tested for mercury absorption, the framework of compound **3** shows excellent ability on absorption of mercury at 150 °C. A temporary explanation is that the framework of **3** has open metal sites and appropriate pore openings for mercury absorption.

CHAPTER V

Syntheses, structures and properties of new MOFs: $[Cu(BrBDC)_2](TEA)_2$ and $Co_2(BrBDC)(HCOO)_2(DMF)_2$, and $Zn_2(BrBDC)(Trz)_2 \cdot 3H_2O$

5.1 Introduction

Based on the results of the mercury adsorption study on selected known MOFs, the next step was to design and synthesize new porous MOFs with appropriate pore openings and open metal sites for mercury absorption. So far the most effective porous material for element mercury removal is powdered activated carbon, especially those impregnated with halogens, which can act as active sites for capturing mercury species.[68] Based on the fact that MOF materials share similar absorption properties with other porous materials, MOFs impregnated with halogen may provide the potential for improving the mercury absorption. Furthermore, halogen could increase the polarizability of the organic linker.[69] In this chapter, we focused on the synthesis of new MOFs using ligands containing halogen functional groups. We chose 2,5-dibromoterepthalic acid (BrBDC) as the main ligand for MOF synthesis because it contains two carboxylate groups that can bind to metal ions and secondary groups for possible mercury absorption. In addition to using one ligand in the synthesis of MOFs, another approach we used to make new MOFs is to use mixed ligands in a synthesis. Three new MOF materials were synthesized based on these ideas: 2D

structure MOFs, $[Cu(BrBDC)_2](TEA)_2$ (TEA=triethylamine, **4**) and $Co_2(BrBDC)(HCOO)_2(DMF)_2$ (**5**), and 3D MOF $Zn_2(BrBDC)(Trz)_2 \cdot 3H_2O$ (Trz=1,2,4-triazole, **6**). Detailed structural analyses with full characterization including X-ray diffraction, infrared spectra, thermogravimetric analyses, and elemental analyses are illustrated**.**

5.2 Synthesis

*5.2.1 Synthesis of $[Cu(BrBDC)_2](HTEA)_2$ (**4**)*

0.154 g $Cu(CH_3COO)_2 \cdot H_2O$ was mixed with 0.500 g 2,5-dibromoterepthalic acid and 0.220 mL triethylamine (TEA) in 1.0 mL methanol. The reaction mixture was transferred to a 3"×4" Teflon bag, which was then sealed and placed in a 45ml Teflon-lined autoclave. The autoclave was placed in an oven and was heated up to 90°C in 12 hours, kept at 90°C for 12 hours, then cooled to 30°C in 18 hours. The resulting products were then filtered using a vacuum filtration system and washed with methanol. Blue crystals of compound 4 were obtained in 48.3% yield (0.340 g). Anal. Calcd for $[Cu(BrBDC)_2](HTEA)_2$

*5.2.2. Synthesis of $Co_2(BrBDC)(HCOO)_2(DMF)_2$ (**5**)*

A mixture of 2,5-dibromoterepthalic (0.0770 g; 0.238 mmol), formic acid (0.0210 g; 0.450 mmol), $Co(NO_3)_2 \cdot 6H_2O$ (0.138 g; 0.474 mmol) and 4.0 mL DMF was placed in a 3"×4" Teflon bag. The bag was sealed and placed in a 45ml Teflon-line autoclave. The autoclave was then placed in an oven programmed and heated at 150 °C for 24 hours.

After cooled naturally, the products were filtered and washed with DI water. Pink crystals were obtained in 74.2% yield (0.119g)

*5.2.3. Synthesis of $Zn_2(BrBDC)(Trz)_2 \cdot 3H_2O$ (**6**)*

Zinc nitrate hexahydrate (0.600 g, 2.00 mmol), BrBDC (0.330g, 1.00 mmol), 1,2,4-triazloe (0.0700 g, 0.00100 mol) and TEA (0.110g, 1.00 mmol) in 2:1:1:1 mole ratio were mixed with 3.6 ml DI water in a 45 mL Teflon cup. The mixture was stirred with a magnetic bar for 1h. Then the Teflon cup was sealed in an autoclave and heated at 150°C for 72h. After cooling to room temperature, the products were filtered and washed with deionized water, dried in air overnight. The product contain yellow crystals of **4** and colorless crystals whose structure is known. The yellow crystals are manually selected for further analysis. The crystal data of **4** is shown in table 5.1.

5.3 Results and Discussion of $[Cu(BrBDC)_2](TEA)_2$ (4)

5.3.1 Description of crystal Structure of $[Cu(BrBDC)_2](HTEA)_2$ (4)

a)

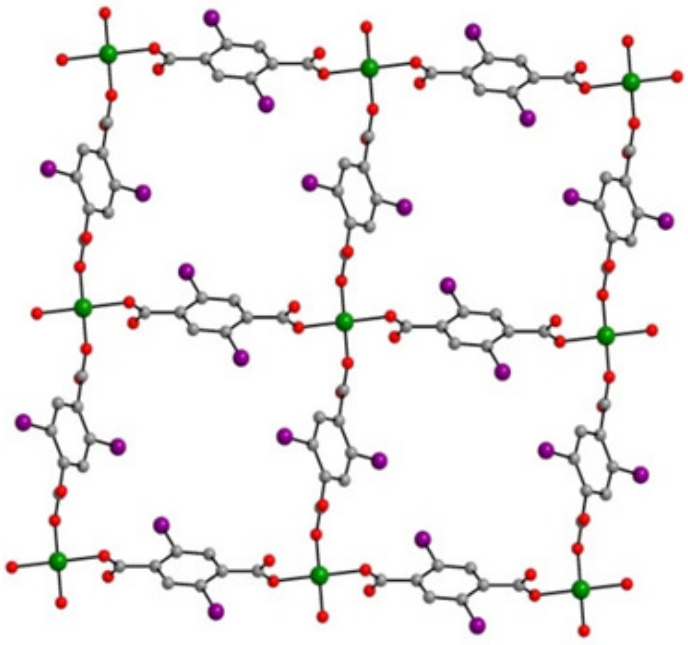

b)

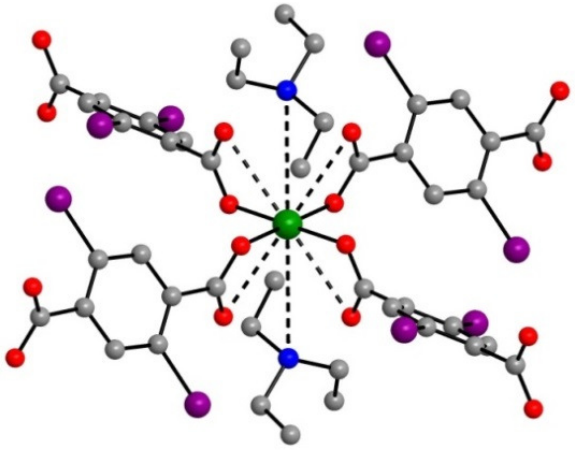

Figure 5.1. (a) Two dimensional structure of $[Cu(BrBDC)_2](TEA)_2$ (**4**). (b) Coordination environment of copper grey: C; Purple: Br; Green: Cu; Red: O; Blue: N.

As shown in Figure 5.1(a), each copper metal ion connects to four other metal ions through four Br_2BDC ligands to form a negatively charged 2D network. The $HTEA^+$ counter ions are located in between the layers. Moreover, as there is a hydrogen atom bonded to the nitrogen of the HTEA+, it is a charged ammonium ion. Thus, the interaction between Cu(II) and the $HTEA^+$ ion is mainly ionic. Compound 4 can also be viewed as an uninodal 4-connected net with a *point symbol* of $(4^4,6^2)$ according to the topological analysis using TOPOS40 program. The crystal structure of compound 4 is 2-D, in P-1(2) space group with triclinic crystal system.[70] The bond angles surrounding copper are 90.776° and 89.224°. The four carboxylate groups coordinated to each copper are in two planes which are almost perpendicular to each other (88.20(6)°). The copper ion also shows to have weak interactions with four oxygen atoms of the carboxylate groups coordinated to it (shows in figure 5-1 (b) with dash line: Cu···O contact: 2.904Å×2 and 2.898 Å×2). [71] In this compound, each carboxylate groups are not coplanar with the benzene ring of the ligand. The dihedral angle is 43.0(1) °. This could be caused by the hydrogen bonds between the Br_2BDC ligand and the $HTEA^+$ ion. Using copper(II) chloride as the source of copper, a new phase $[Cu(Cl_2BDC)_2](HTEA)_2$ (Cl_2BDC = 2,5-dichloroterepthalic acid) was isolated from the products. This compound is isostructural to compound **4**. The stacking of the layers forms one-dimensional channels of *ca* 5.8×6.4 Å along the *b* direction, with the counter ions in the channels.

Table 5.1 Crystallographic data for $[Cu(BrBDC)_2](TEA)_2$ **(4)**

Formula	C28H36Br4CuN2O8
Mol. wt	911.77
Crystal system	Triclinic
Space group	$P\bar{1}$
a(Å)	9.0470(7)
b(Å)	9.9015(8)
c(Å)	10.9860(9)
α(°)	76.252(4)
β(°)	68.805(3)
γ(°)	69.874(4)
V($Å^3$)	854.3(1)
Z	1
ρ (Mg/m^3)	1.772
μ (mm^{-1})	5.364
Wavelength(Å)	0.71073
Temperature(K)	296
Reflections collected/unique	6841[0.0215]
Goodness-of-fit(F^2)	0.997
Final R indices [$I > 2\sigma(I)$]	R_1=0.0321, wR_2=0.0668
R indices (all data)	R_1=0.0513, wR_2=0.0729

5.3.2 Thermal Stabilities of [Cu(BrBDC)$_2$](HTEA)$_2$ (4)

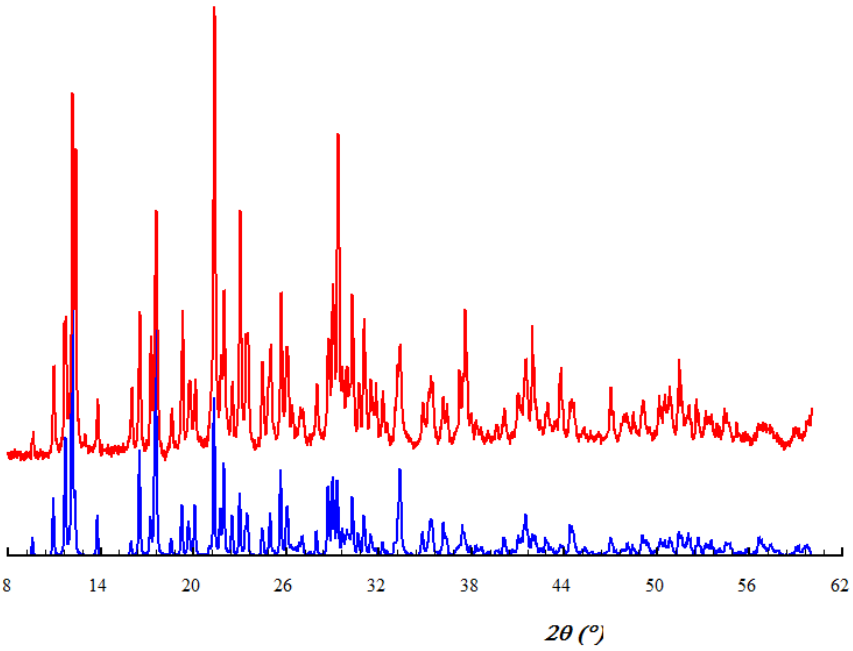

Figure 5.2. PXRD patterns of [Cu(BrBDC)$_2$](TEA)$_2$ (**4**). Blue: simulated from SXRD; red: experimental.

The purity of the bulk sample was examined by PXRD. As shown in Figure 5.2, the experimental PXRD pattern of 4 agree very well with that of simulated from the single crystal structure. This indicates the synthesized sample of 4 is pure.

*5.3.3 Thermogravimetric Analysis of [Cu(BrBDC)$_2$](HTEA)$_2$ (**4**)*

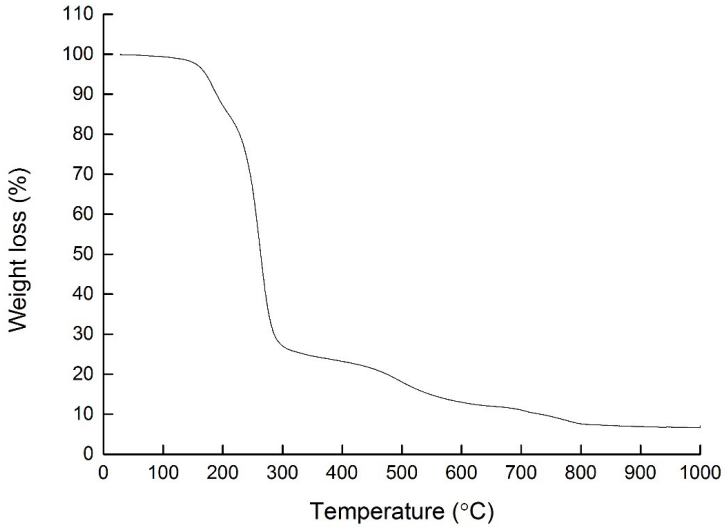

Figure 5.3. TGA pattern of $[Cu(BrBDC)_2](TEA)_2$ (**4**).

The TGA plot of **3** is shown in Figure 5.3. Between 120 °C and 360 °C, a total weight loss of 75.7% is recorded. This includes a weight loss of 21.3% at 120-230 °C, which can be attributed to the removal of $HTEA^+$ (cal 22.42%). The decomposition of the Br_2BDC ligand occurs at 230 °C.

5.3.4 FTIR pattern of $[Cu(BrBDC)_2](HTEA)_2$ (4)

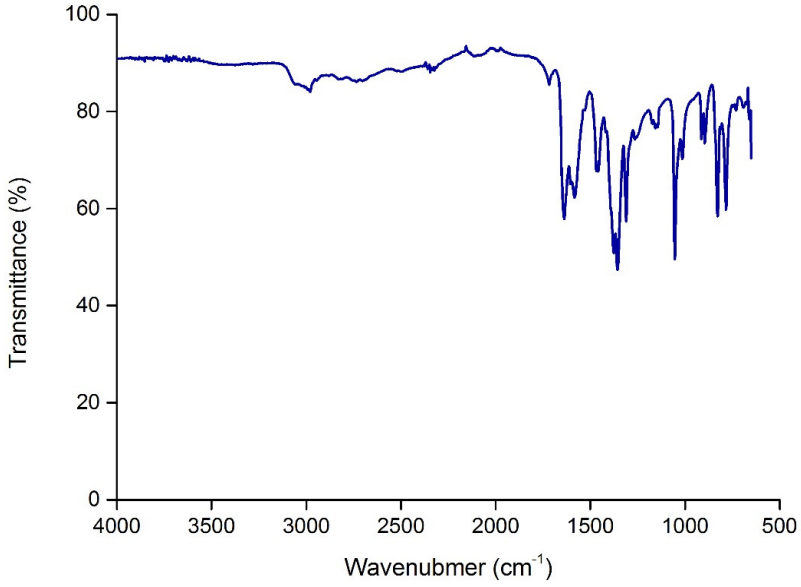

Figure 5.4. The IR spectra for $[Cu(BrBDC)_2](TEA)_2$ (**4**).

The FTIR spectra of compound 4 are shown in figure 5-4. The band at 1638 cm^{-1} is the C=O vibration and the band at 1584 cm^{-1} is from C=C of the benzene ring.

5.4 Results and discussion of $Co_2(BrBDC)(COO)_2(DMF)_2$ (5)

*5.4.1 Structure Description of $Co_2(BrBDC)(COO)_2(DMF)_2$ (**5**)*

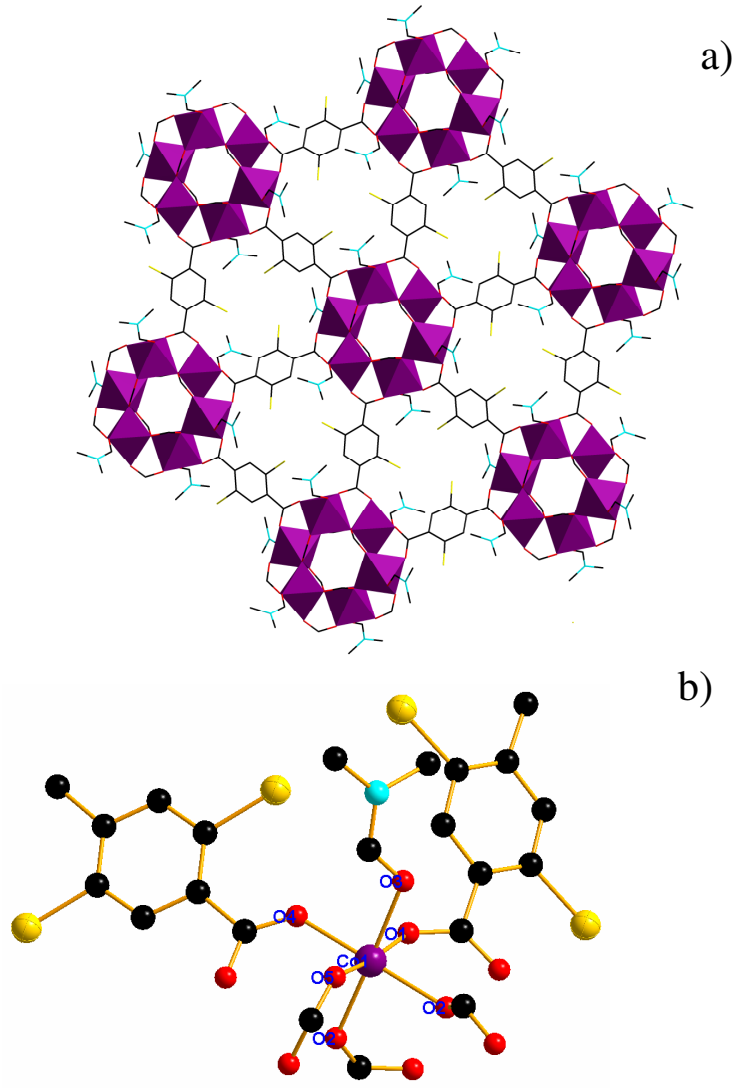

Figure 5.5. (a) Two dimensional structure of $Co_2(BrBDC)(COO)_2(DMF)_2$ (**5**). (b) Coordination environment of cobalt Red: O; Purple: Co; Black: C; Cyan: N; Yellow: Br.

Compound **5** was initially synthesized from BTC, cobalt nitrate and BrBDC under solvothermal conditions. However, BTC was not found in the structure of **5**. Instead, $HCOO^-$ was found to coordinate to Co(II) in the structure. We then used formic acid to replace BTC in the synthesis and successfully made compound **5**. It is known that carboxylate groups on aromatic rings are unstable and may be removed under solvothermal conditions. Decarboxylate was observed for similar ligands such as 1,2,4-triazole-3-carboxylic acid.[72] 3-amino-1,2,4-triazole-5-carboxylic acid[73], and 1,2,3-benzenetricarboxylic acid.[73-74] Normally, after one or more carboxylate groups were removed, the residue of the ligand would incorporate into the resulting structures. However, in **5**, the removed carboxylate coordinates to the cobalt ions. It is believe that the decarboxylate procedure requires the high temperature and basic condition.[74] However, we did not add bases to the reaction mixture in the synthesis of **5**.

The structure of compound **5** consists of a layered network built from cobalt ions and organic ligands. The cobalt(II) ion exhibits an octahedral coordination geometry and is six-coordinated to three formate ions, two Br_2BDC ligand ions, and one DMF molecule. Six Co-O octahedron form a cluster, three this kind of cluster occupy vertex form a triangle connected by 2,5-dibrBDC. So, there are two types of hexagonal pores. One is formed by the six CoO_6 polyhedral, the other one is the central of the triangle. The Co-O bond lengths range from 2.054(1)Å to 2.127(1) Å. Each Br_2BDC, as a tetradentate ligand, binds to four cobalt ions through its carboxylate groups.[75] The cluster is dangled with six Br_2BDC ligands to form a pedal, wheel.

The pedal wheel building units are connected by sharing their the Br_2BDC ligands into a 2D layered networks. The stacking of the layers along the c direction forms one-dimensional channels.[76]

Table 5.2 Crystallographic data for $Co_2(BrBDC)(COO)_2(DMF)_2$ **(5)**

Formula	$C_8H_9BrCoNO_5$
Mol. wt	338.00
Crystal system	Hexagonal
Space group	$P\bar{3}$
a(Å)	16.046(1)
b(Å)	16.046(1)
c(Å)	7.6321(9)
α(°)	90.00
β(°)	90.00
γ(°)	120.00
V(Å^3)	1701.8(3)
Z	6
ρ (Mg/m^3)	1.979
μ (mm^{-1})	5.038
Wavelength(Å)	0.71073
Temperature(K)	296
Reflections collected/unique	4820[0.0382]
Goodness-of-fit(F^2)	1.041
Final R indices [I > 2σ(I)]	R_1=0.0299, wR_2= 0.0700
R indices (all data)	R_1=0.0392, wR_2= 0.0749

5.4.2 Thermal Stabilities of $Co_2(BrBDC)(COO)_2(DMF)_2$ (5)

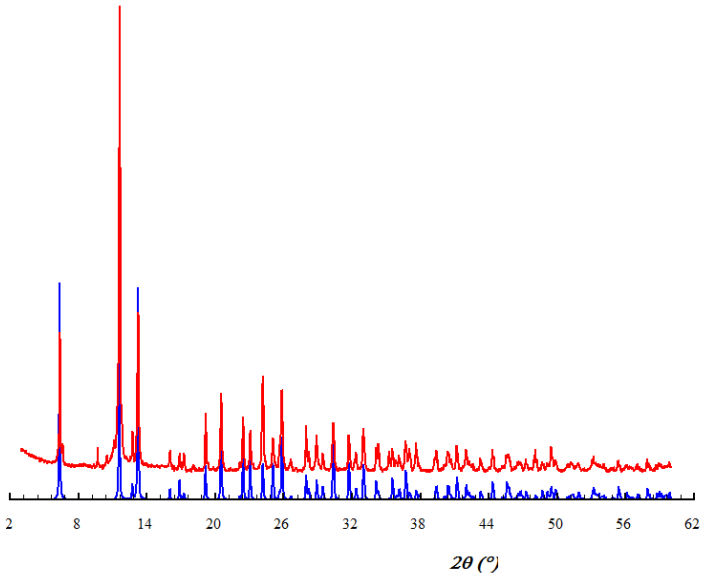

Figure 5.6 XRD patterns of $Co_2(BrBDC)(COO)_2(DMF)_2$(**4**)**.** Blue: simulated from SXR; red experimental.

The purity of the sample has been confirmed by the PXRD analysis of **5**. As shown in the figure 5.6, experimental PXRD patterns and those of simulated PXRD pattern from the single crystal structures match very well.

5.4.3 Thermogravimetric Analysis of $Co_2(BrBDC)(HCOO)_2(DMF)_2$ (5)

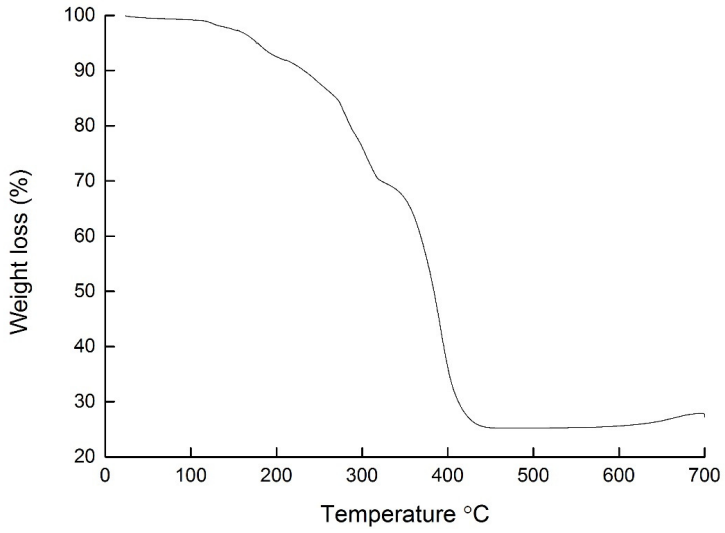

Figure 5.7. TGA plot of $Co_2(BrBDC)(COO)_2(DMF)_2$ (**4**)**.**

The TGA plot of **5** shows a total weight loss of 29.9% begin at around 130°C up to 350°C, which can be attributed to the removal of DMF. The next weight loss is due to the decomposition and removal of organic ligands. The second weight loss between 350-460°C is 34.7%.

5-4-4 FTIR of $Co_2(BrBDC)(COO)_2(DMF)_2$ (5)

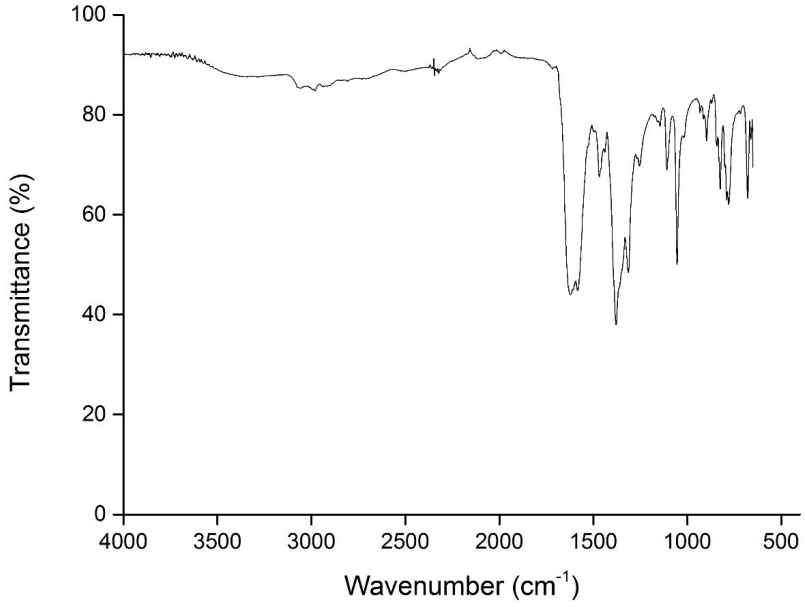

Figure 5.8. The IR spectra for $Co_2(BrBDC)(COO)_2(DMF)_2$ (**4**)**.**

The IR spectra of **5** show vibrational bands in the range of 1620–1550 cm^{-1} corresponding to the stretching vibrations of the carboxylic groups.[77] The absorptions at 1400–1363 cm^{-1} are the characteristic bands of the symmetric vibrations of carboxylic groups.[78] The lack of absorption of characteristic of any protonated forms if carboxylic groups between (1715–1680 cm-1) or (1730–1690 cm-1) manifest the complete deprotonation of the BrBDC ligand or formate ligand.

5.5. Results and discussion of $Zn_2(BrBDC)(Trz)_2 \cdot 3H_2O$ (6)

5.5.1 Description of Crystal Structure of $Zn_2(BrBDC)(Trz)_2 \cdot 3H_2O$ (6)

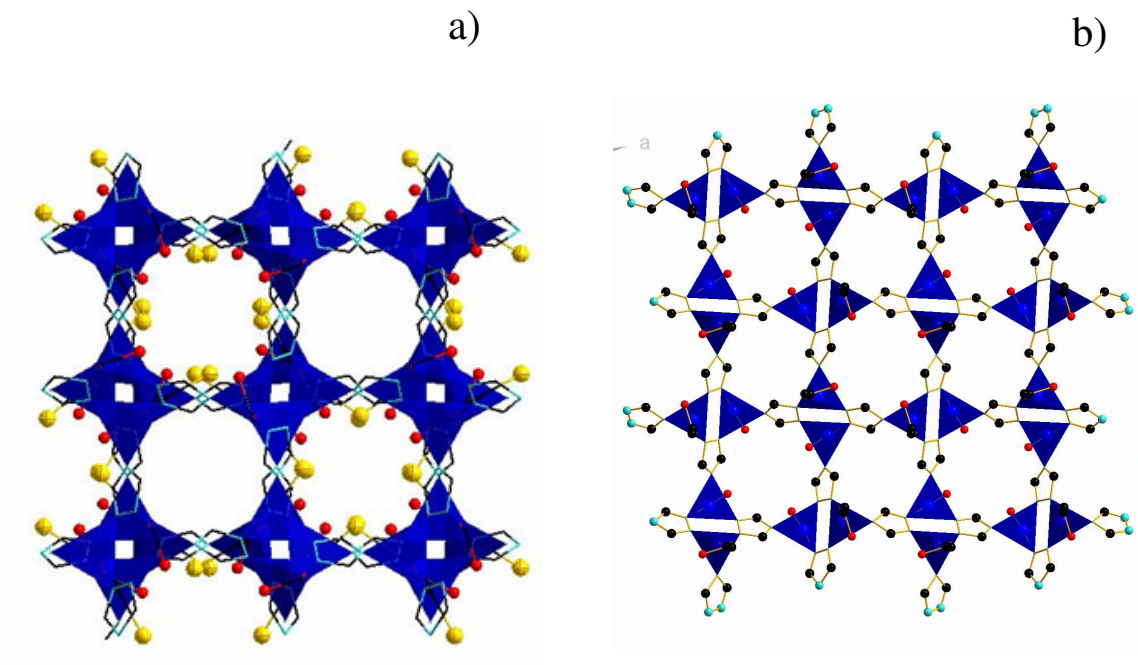

Figure 5.9 (a) Three dimensional Structure of $Zn_2(BrBDC)(Trz)_2 \cdot 3H_2O$ (**6**), (b) 8-membered ring formed by Zn dimer. Black: C; Yellow: Br; Red: O; Blue: Zn; Cyan: N.

Single-crystal X-ray diffraction analysis reveals that **6** crystallizes in the tetragonal system and its space group is P4 (75). Compound 6 couldn't be made if TEA is not used in the reaction mixture. This could be caused by the fact that 1,2,4-triazole molecule only can coordinate into open framework under deprotonated form.[79,80] There are four unique Zn atoms in the asymmetric unit. Each of them has the same coordination form and coordination number. Three of coordination ligands of the Zn atom are 1,2,4-triazole molecules. The fourth ligand of Zn is O atom from the carboxylate group. Zn1 and Zn4 connect to each other into a dimer through two Trz molecules to form an eight-membered ring (figure 5-9 (b)). Zn5 and Zn6 are located at adjacent layers, which are

connected by BrBDC ligands. The 3D framework of 6 contains 1D channels along the c axis (figure 5-9 (a)). A compound with similar crystal structure to 6 has been reported by Hyunsoo Park's.[81]

Table 5.3 Crystallographic data for $Zn_2(BrBDC)(Trz)_2 \cdot 3H_2O$ (6)

Formula	$C_{48}H_{40}Br_8N_{24}O_{28}Zn_8$
Mol. wt	2563.28
Crystal system	tetragonal
Space group	P4/ncc
a(Å)	13.4824(3)
b(Å)	13.4824(3)
c(Å)	27.0886(5)
α(°)	90°
β(°)	90°
γ(°)	90°
V(Å^3)	4923.92(18) Å^3
Z	2
ρ (Mg/m^3)	1.729
μ (mm^{-1})	5.233
Wavelength(Å)	0.71073 Å
Temperature(K)	569(2) K
Reflections collected/unique	112955
[R_{int}]	0.0730
Goodness-of-fit(F^2)	1.132
Final R indices [I > 2σ(I)]	R1 = 0.1068, wR2 = 0.3145
R indices (all data)	R1 = 0.1326, wR2 = 0.3474

5.5.2 Thermal Stabilities of $Zn_2(BrBDC)(Trz)_2 \cdot 3H_2O$ (6)

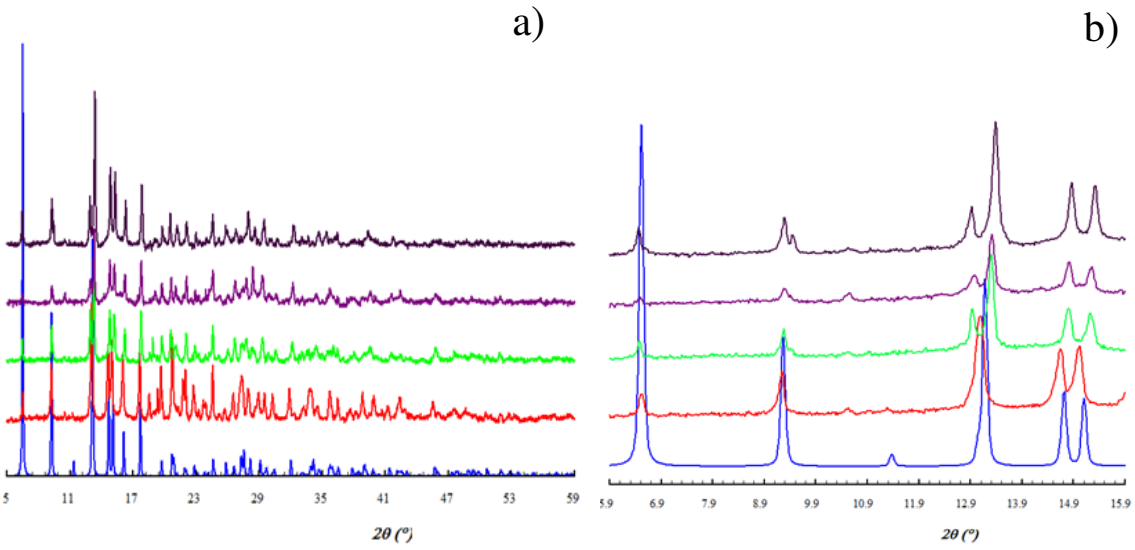

Figure 5.10. (a) Thermal stabilities of $Zn_2(BrBDC)(Trz)_2 \cdot 3H_2O$ (**6**). Blue: simulated from SXRD; red: experimental; green: heated at 150℃ for 12h; purple: heated at 180℃ for 12h; black: heated at 210℃ for 12h. (b) Partial enlarged patterns between angle 5.9° and 15.9°.

The PXRD pattern of synthesized sample of **6** matches well with the simulated PXRD pattern from the single crystal structure of **6**, indicating the sample of **6** is pure. After heated at over 150 ℃, some peaks showed a slightly shift to high angles in comparison with the unheated sample. This can be attributed to the departure of the water resulting in the decrease of the cell unit parameters.[82] However, the framework of **6** did not collapse indicating the flexibility of the framework, which is not common in Zn triazolate-dicarboxylate pillared-layer MOFs.[83]

*5.5.3 Thermal-gravimetric Analysis of $Zn_2(BrBDC)(Trz)_2 \cdot 3H_2O$ (**6**)*

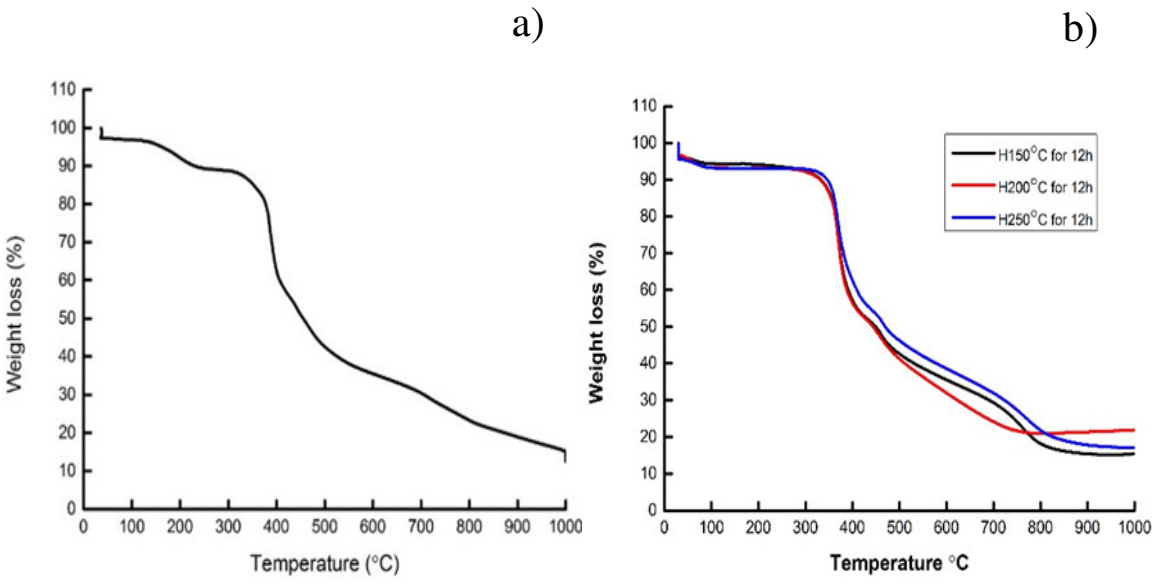

Figure 5.11. a) TGA plot of $Zn_2(BrBDC)(Trz)_2 \cdot 3H_2O$ (**6**)**.** (b) TGA plots of 6 after heated at 150℃, 180℃ and 210℃ kept for 12h.

Figure 5.11 (a) shows the TGA plot of **6**. The weight loss occurred from room temperature to 220°C corresponds to 3 units of water molecules. As can be seen from Figure 5.11b, the water molecules in channels of the framework of 6 can be removed by heating the samples of 6 in an oven for 12 hours.

5.5.4 FTIR of $Zn_2(BrBDC)(Trz)_2 \cdot 3H_2O$ (6)

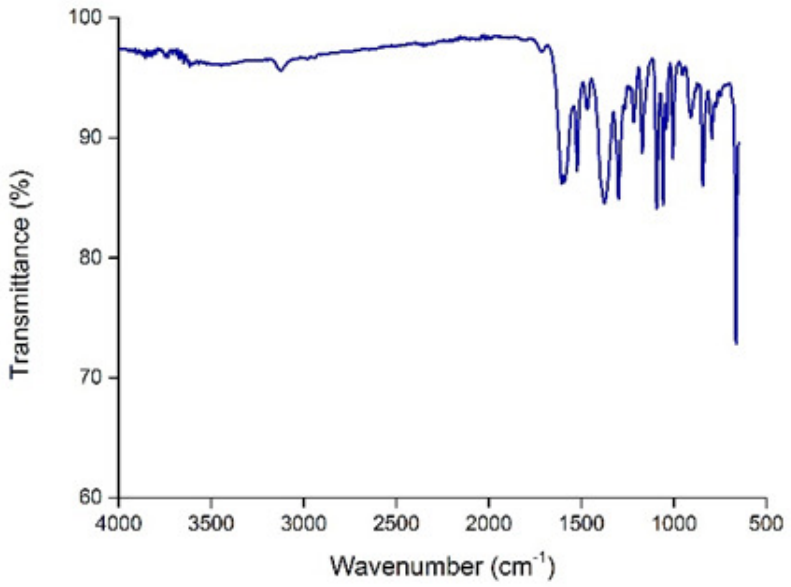

Figure 5.12. The IR spectra of $Zn_2(BrBDC)(Trz)_2 \bullet 3H_2O$ (**6**).

As shown in Figure 5.12, at the IR band at 1060 cm^{-1} can be attributed to C-O deformation. The band at 1601 cm^{-1} is associated with stretching vibrations of the C=O bond. The band at 1700 cm^{-1} was assigned to the stretching vibrations of the C-O bond. The bands in range of 700 cm^{-1} to 1200 cm^{-1} can be assigned to C-H and C-C bending of the benzene ring. The small peak at around 3200 cm^{-1}.[84] corresponds to O-H group of water molecule.[82c]

5.6 Conclusions

Three new metal-organic frameworks have been hydrothermally synthesized using transition metal ions and the 2,5-dibromoterepthalate ligand. The structure of **4** consists of anionic layered networks balanced with cationic $HTEA^+$ ions located in between the layers. While the structure of **5** is a neutral 2D coordination network containing

hexagonal rings of clusters formed by six CoO_6 octahedra. Compound **6** is a 3D open framework with one-dimensional channels.

REFERENCES

1. Ramesh, G. V.; Radhakrishnan, T. P., A Universal Sensor for Mercury (Hg, HgI, HgII) Based on Silver Nanoparticle-Embedded Polymer Thin Film. *ACS applied materials & interfaces* **2011,** *3* (4), 988-994.

2. Presto, A. A.; Granite, E. J., Noble Metal Catalysts for Mercury Oxidation in Utility Flue Gas. *Platinum Metals Review* **2008,** *52* (3), 144-154.

3. Suh, M. P.; Park, H. J.; Prasad, T. K.; Lim, D. W., Hydrogen storage in metal-organic frameworks. *Chemical reviews* **2012,** *112* (2), 782-835.

4. YAN LIU, D. J. A. K.; HONGQUN YANG; CHRISTOPHER C. H. LIN; STEVE M. KUZNICKI, A. Z. X., Novel Regenerable Sorbent for Mercury Capture from Flue Gases of Coal-Fired Power Plant. *Environ. Sci. Technol.* **2008,** *42*, 6205-6210.

5. (a) Karatza, D.; Lancia, A.; Prisciandaro, M.; Musmarra, D.; Mazziotti di Celso, G., Influence of oxygen on adsorption of elemental mercury vapors onto activated carbon. *Fuel* **2013,** *111*, 485-491; (b) Huang, Y.; Jin, B.; Zhong, Z.; Xiao, R.; Tang, Z.; Ren, H., Trace elements (Mn, Cr, Pb, Se, Zn, Cd and Hg) in emissions from a pulverized coal boiler. *Fuel Processing Technology* **2004,** *86* (1), 23-32.

6. Furukawa, H.; Cordova, K. E.; O'Keeffe, M.; Yaghi, O. M., The chemistry and applications of metal-organic frameworks. *Science* **2013,** *341* (6149), 1230444.

7. (a) Tranchemontagne, D. J.; Park, K. S.; Furukawa, H.; Eckert, J.; Knobler, C. B.; Yaghi, O. M., Hydrogen Storage in New Metal–Organic Frameworks. *The Journal of Physical Chemistry C* **2012,** *116* (24), 13143-13151; (b) Mendoza-Cortes, J. L.; Goddard,

W. A.; Furukawa, H.; Yaghi, O. M., A Covalent Organic Framework that Exceeds the DOE 2015 Volumetric Target for H2Uptake at 298 K. *The Journal of Physical Chemistry Letters* **2012,** *3* (18), 2671-2675; (c) Nguyen Thi, T. V.; Luu, C. L.; Hoang, T. C.; Nguyen, T.; Bui, T. H.; Duy Nguyen, P. H.; Pham Thi, T. P., Synthesis of MOF-199 and application to CO2adsorption. *Advances in Natural Sciences: Nanoscience and Nanotechnology* **2013,** *4* (3), 035016.

8. Ma, S.; Sun, D.; Wang, X. S.; Zhou, H. C., A mesh-adjustable molecular sieve for general use in gas separation. *Angewandte Chemie* **2007,** *46* (14), 2458-62.

9. (a) Keskin, S.; Kızılel, S., Biomedical Applications of Metal Organic Frameworks. *Industrial & Engineering Chemistry Research* **2011,** *50* (4), 1799-1812; (b) Liédana, N.; Galve, A.; Rubio, C.; Téllez, C.; Coronas, J., CAF@ZIF-8: One-Step Encapsulation of Caffeine in MOF. *ACS applied materials & interfaces* **2012,** *4* (9), 5016-5021.

10. (a) Choi, S.; Watanabe, T.; Bae, T.-H.; Sholl, D. S.; Jones, C. W., Modification of the Mg/DOBDC MOF with Amines to Enhance CO2 Adsorption from Ultradilute Gases. *The Journal of Physical Chemistry Letters* **2012,** *3* (9), 1136-1141; (b) Shultz, A. M.; Farha, O. K.; Hupp, J. T.; Nguyen, S. T., A Catalytically Active, Permanently Microporous MOF with Metalloporphyrin Struts. *Journal of the American Chemical Society* **2009,** *131* (12), 4204-4205.

11. Yaghi, O. M., Metal-organic Frameworks: A tale of two entanglements. *Nature materials* **2007,** *6* (2), 92-93.

12. Fracaroli, A. M.; Furukawa, H.; Suzuki, M.; Dodd, M.; Okajima, S.; Gandara, F.; Reimer, J. A.; Yaghi, O. M., Metal-organic frameworks with precisely designed interior

for carbon dioxide capture in the presence of water. *J Am Chem Soc* **2014,** *136* (25), 8863-6.

13. Gandara, F.; Furukawa, H.; Lee, S.; Yaghi, O. M., High methane storage capacity in aluminum metal-organic frameworks. *J Am Chem Soc* **2014,** *136* (14), 5271-4.

14. (a) Shultz, A. M.; Sarjeant, A. A.; Farha, O. K.; Hupp, J. T.; Nguyen, S. T., Post-Synthesis Modification of a Metal–Organic Framework To Form Metallosalen-Containing MOF Materials. *Journal of the American Chemical Society* **2011,** *133* (34), 13252-13255; (b) Crees, R. S.; Cole, M. L.; Hanton, L. R.; Sumby, C. J., Synthesis of a Zinc(II) Imidazolium Dicarboxylate Ligand Metal−Organic Framework (MOF): a Potential Precursor to MOF-Tethered N-Heterocyclic Carbene Compounds. *Inorganic chemistry* **2010,** *49* (4), 1712-1719.

15. Li, J. R.; Sculley, J.; Zhou, H. C., Metal-organic frameworks for separations. *Chemical reviews* **2012,** *112* (2), 869-932.

16. Activated Carbon Adsorption from Solutions. In *Activated Carbon Adsorption*, CRC Press: 2005; pp 145-199.

17. (a) Stock, N.; Biswas, S., Synthesis of metal-organic frameworks (MOFs): routes to various MOF topologies, morphologies, and composites. *Chemical reviews* **2012,** *112* (2), 933-69; (b) Biradha, K.; Ramanan, A.; Vittal, J. J., Coordination Polymers Versus Metal−Organic Frameworks. *Crystal Growth & Design* **2009,** *9* (7), 2969-2970.

18. Hoskins, B. F.; Robson, R., Design and construction of a new class of scaffolding-like materials comprising infinite polymeric frameworks of 3D-linked molecular rods. A reappraisal of the zinc cyanide and cadmium cyanide structures and the synthesis and structure of the diamond-related frameworks [N(CH3)4][CuIZnII(CN)4]

and CuI[4,4',4",4"'-tetracyanotetraphenylmethane]BF4.xC6H5NO2. *Journal of the American Chemical Society* **1990,** *112* (4), 1546-1554.

19. Li, H.; Eddaoudi, M.; O'Keeffe, M.; Yaghi, O. M., Design and synthesis of an exceptionally stable and highly porous metal-organic framework. *Nature* **1999,** *402* (6759), 276-279.

20. Chui, S. S.-Y.; Lo, S. M.-F.; Charmant, J. P. H.; Orpen, A. G.; Williams, I. D., A Chemically Functionalizable Nanoporous Material [Cu3(TMA)2(H2O)3]n. *Science* **1999,** *283* (5405), 1148-1150.

21. Eddaoudi, M.; Kim, J.; Rosi, N.; Vodak, D.; Wachter, J.; O'Keeffe, M.; Yaghi, O. M., Systematic Design of Pore Size and Functionality in Isoreticular MOFs and Their Application in Methane Storage. *Science* **2002,** *295* (5554), 469-472.

22. Cohen, S. M., Postsynthetic methods for the functionalization of metal-organic frameworks. *Chemical reviews* **2012,** *112* (2), 970-1000.

23. (a) Dybtsev, D. N.; Chun, H.; Kim, K., Rigid and Flexible: A Highly Porous Metal–Organic Framework with Unusual Guest-Dependent Dynamic Behavior. *Angewandte Chemie International Edition* **2004,** *43* (38), 5033-5036; (b) Seki, K.; Mori, W., Syntheses and Characterization of Microporous Coordination Polymers with Open Frameworks. *The Journal of Physical Chemistry B* **2002,** *106* (6), 1380-1385.

24. Ma, S., Gas adsorption applications of porous metal–organic frameworks. *Pure and Applied Chemistry* **2009,** *81* (12).

25. (a) Zeng, Y. F.; Hu, X.; Liu, F. C.; Bu, X. H., Azido-mediated systems showing different magnetic behaviors. *Chemical Society reviews* **2009,** *38* (2), 469-80; (b)

Kurmoo, M., Magnetic metal-organic frameworks. *Chemical Society reviews* **2009,** *38* (5), 1353-1379.

26. Allendorf, M. D.; Bauer, C. A.; Bhakta, R. K.; Houk, R. J. T., Luminescent metal-organic frameworks. *Chemical Society reviews* **2009,** *38* (5), 1330-1352.

27. García-Pérez, E.; Gascón, J.; Morales-Flórez, V.; Castillo, J. M.; Kapteijn, F.; Calero, S., Identification of Adsorption Sites in Cu-BTC by Experimentation and Molecular Simulation. *Langmuir* **2009,** *25* (3), 1725-1731.

28. Song, Y. F.; Cronin, L., Postsynthetic covalent modification of metal-organic framework (MOF) materials. *Angewandte Chemie* **2008,** *47* (25), 4635-7.

29. Lu, W.; Wei, Z.; Gu, Z. Y.; Liu, T. F.; Park, J.; Park, J.; Tian, J.; Zhang, M.; Zhang, Q.; Gentle, T., 3rd; Bosch, M.; Zhou, H. C., Tuning the structure and function of metal-organic frameworks via linker design. *Chemical Society reviews* **2014,** *43* (16), 5561-93.

30. Braun, M. E.; Steffek, C. D.; Kim, J.; Rasmussen, P. G.; Yaghi, O. M., *Chemical communications* **2001,** (24), 2532-2533.

31. Wang, Z.; Cohen, S. M., Postsynthetic modification of metal-organic frameworks. *Chemical Society reviews* **2009,** *38* (5), 1315-29.

32. Park, H. J.; Cheon, Y. E.; Suh, M. P., Post-synthetic reversible incorporation of organic linkers into porous metal-organic frameworks through single-crystal-to-single-crystal transformations and modification of gas-sorption properties. *Chemistry* **2010,** *16* (38), 11662-9.

33. Han, S. S.; Goddard, W. A., Lithium-Doped Metal-Organic Frameworks for Reversible H2 Storage at Ambient Temperature. *Journal of the American Chemical Society* **2007,** *129* (27), 8422-8423.

34. Pachfule, P.; Das, R.; Poddar, P.; Banerjee, R., Solvothermal Synthesis, Structure, and Properties of Metal Organic Framework Isomers Derived from a Partially Fluorinated Link. *Crystal Growth & Design* **2011,** *11* (4), 1215-1222.

35. (a) Forster, P. M.; Stock, N.; Cheetham, A. K., A high-throughput investigation of the role of pH, temperature, concentration, and time on the synthesis of hybrid inorganic-organic materials. *Angewandte Chemie* **2005,** *44* (46), 7608-11; (b) Bauer, S.; Stock, N., Implementation of a temperature-gradient reactor system for high-throughput investigation of phosphonate-based inorganic-organic hybrid compounds. *Angewandte Chemie* **2007,** *46* (36), 6857-60.

36. Cravillon, J.; Münzer, S.; Lohmeier, S.-J.; Feldhoff, A.; Huber, K.; Wiebcke, M., Rapid Room-Temperature Synthesis and Characterization of Nanocrystals of a Prototypical Zeolitic Imidazolate Framework. *Chemistry of Materials* **2009,** *21* (8), 1410-1412.

37. Stock, N.; Biswas, S., Synthesis of Metal-Organic Frameworks (MOFs): Routes to Various MOF Topologies, Morphologies, and Composites. *Chemical reviews* **2011,** *112* (2), 933-969.

38. Liu, Q.; Low, Z.-X.; Li, L.; Razmjou, A.; Wang, K.; Yao, J.; Wang, H., ZIF-8/Zn2GeO4 nanorods with an enhanced CO2 adsorption property in an aqueous medium for photocatalytic synthesis of liquid fuel. *Journal of Materials Chemistry A* **2013,** *1* (38), 11563.

39. Hessel, V.; Löwe, H., Microchemical Engineering: Components, Plant Concepts User Acceptance – Part I. *Chemical Engineering & Technology* **2003,** *26* (1), 13-24.

40. Yoo, Y.; Jeong, H.-K., Rapid fabrication of metal organic framework thin films using microwave-induced thermal deposition. *Chemical communications* **2008,** (21), 2441-2443.

41. Qiu, L.-G.; Li, Z.-Q.; Wu, Y.; Wang, W.; Xu, T.; Jiang, X., Facile synthesis of nanocrystals of a microporous metal-organic framework by an ultrasonic method and selective sensing of organoamines. *Chemical communications* **2008,** (31), 3642-3644.

42. Xu, F.; Xian, S.; Xia, Q.; Li, Y.; Li, Z., Effect of Textural Properties on the Adsorption and Desorption of Toluene on the Metal-Organic Frameworks HKUST-1 and MIL-101. *Adsorption Science & Technology* **2013,** *31* (4), 325-340.

43. Pan, L.; Parker, B.; Huang, X.; Olson, D. H.; Lee; Li, J., Zn(tbip) (H2tbip= 5-tert-Butyl Isophthalic Acid): A Highly Stable Guest-Free Microporous Metal Organic Framework with Unique Gas Separation Capability. *Journal of the American Chemical Society* **2006,** *128* (13), 4180-4181.

44. Pan, L.; Olson, D. H.; Ciemnolonski, L. R.; Heddy, R.; Li, J., Separation of Hydrocarbons with a Microporous Metal–Organic Framework. *Angewandte Chemie International Edition* **2006,** *45* (4), 616-619.

45. Cui, Y.; Yue, Y.; Qian, G.; Chen, B., Luminescent functional metal-organic frameworks. *Chemical reviews* **2012,** *112* (2), 1126-62.

46. Horcajada, P.; Serre, C.; Vallet-Regí, M.; Sebban, M.; Taulelle, F.; Férey, G., Metal–Organic Frameworks as Efficient Materials for Drug Delivery. *Angewandte Chemie International Edition* **2006,** *45* (36), 5974-5978.

47. Yoon, M.; Srirambalaji, R.; Kim, K., Homochiral metal-organic frameworks for asymmetric heterogeneous catalysis. *Chemical reviews* **2012,** *112* (2), 1196-231.

48. Seo, J. S.; Whang, D.; Lee, H.; Jun, S. I.; Oh, J.; Jeon, Y. J.; Kim, K., A homochiral metal-organic porous material for enantioselective separation and catalysis. *Nature* **2000,** *404* (6781), 982-986.

49. (a) Eliseeva, S. V.; Bunzli, J.-C. G., Lanthanide luminescence for functional materials and bio-sciences. *Chemical Society reviews* **2010,** *39* (1), 189-227; (b) Binnemans, K., Lanthanide-Based Luminescent Hybrid Materials. *Chemical reviews* **2009,** *109* (9), 4283-4374; (c) Hwang, S.-H.; Moorefield, C. N.; Newkome, G. R., Dendritic macromolecules for organic light-emitting diodes. *Chemical Society reviews* **2008,** *37* (11), 2543-2557.

50. Fletcher, D. A.; McMeeking, R. F.; Parkin, D., The United Kingdom Chemical Database Service. *Journal of Chemical Information and Computer Sciences* **1996,** *36* (4), 746-749.

51. Ellsworth, J. M.; zur Loye, H.-C., Metal and mixed-metal coordination polymers synthesized with pyrazine-2-carboxylate. *Dalton transactions* **2008,** (43), 5823-5835.

52. Ouellette, W.; Yu, M. H.; O'Connor, C. J.; Hagrman, D.; Zubieta, J., Hydrothermal chemistry of the copper-triazolate system: A microporous metal-organic framework constructed from magnetic {Cu3(mu3-OH)(triazolate)3}2+ building blocks, and related materials. *Angewandte Chemie* **2006,** *45* (21), 3497-500.

53. Tan, J. C.; Bennett, T. D.; Cheetham, A. K., Chemical structure, network topology, and porosity effects on the mechanical properties of Zeolitic Imidazolate

Frameworks. *Proceedings of the National Academy of Sciences* **2010,** *107* (22), 9938-9943.

54. Xiong, Y.; Ye, F.; Zhang, C.; Shen, S.; Su, L.; Zhao, S., Synthesis of magnetic porous [gamma]-Fe2O3/C@HKUST-1 composites for efficient removal of dyes and heavy metal ions from aqueous solution. *RSC Advances* **2015,** *5* (7), 5164-5172.

55. Chen, L.; Grajciar, L.; Nachtigall, P.; Düren, T., Accurate Prediction of Methane Adsorption in a Metal–Organic Framework with Unsaturated Metal Sites by Direct Implementation of an ab Initio Derived Potential Energy Surface in GCMC Simulation. *The Journal of Physical Chemistry C* **2011,** *115* (46), 23074-23080.

56. Darensbourg, D. J.; Chung, W.-C.; Wang, K.; Zhou, H.-C., Sequestering CO2for Short-Term Storage in MOFs: Copolymer Synthesis with Oxiranes. *ACS Catalysis* **2014,** *4* (5), 1511-1515.

57. Yudovich, Y. E.; Ketris, M. P., Mercury in coal: a review Part 2. Coal use and environmental problems. *International Journal of Coal Geology* **2005,** *62* (3), 135-165.

58. Li, K.; Olson, D. H.; Lee, J. Y.; Bi, W.; Wu, K.; Yuen, T.; Xu, Q.; Li, J., Multifunctional Microporous MOFs Exhibiting Gas/Hydrocarbon Adsorption Selectivity, Separation Capability and Three-Dimensional Magnetic Ordering. *Advanced Functional Materials* **2008,** *18* (15), 2205-2214.

59. Hsi, H.-C.; Chen, S.; Rostam-Abadi, M.; Rood, M. J.; Richardson, C. F.; Carey, T. R.; Chang, R., Preparation and Evaluation of Coal-Derived Activated Carbons for Removal of Mercury Vapor from Simulated Coal Combustion Flue Gases. *Energy & Fuels* **1998,** *12* (6), 1061-1070.

60. Choi, E.-Y.; Wray, C. A.; Hu, C.; Choe, W., Highly tunable metal-organic frameworks with open metal centers. *CrystEngComm* **2009,** *11* (4), 553-555.

61. (a) Tian, Y. Q.; Zhao, Y. M.; Chen, Z. X.; Zhang, G. N.; Weng, L. H.; Zhao, D. Y., Design and generation of extended zeolitic metal-organic frameworks (ZMOFs): synthesis and crystal structures of zinc(II) imidazolate polymers with zeolitic topologies. *Chemistry* **2007,** *13* (15), 4146-54; (b) Tian, Y. Q.; Cai, C. X.; Ren, X. M.; Duan, C. Y.; Xu, Y.; Gao, S.; You, X. Z., The silica-like extended polymorphism of cobalt(II) imidazolate three-dimensional frameworks: X-ray single-crystal structures and magnetic properties. *Chemistry* **2003,** *9* (22), 5673-85.

62. Park, K. S.; Ni, Z.; Cote, A. P.; Choi, J. Y.; Huang, R.; Uribe-Romo, F. J.; Chae, H. K.; O'Keeffe, M.; Yaghi, O. M., Exceptional chemical and thermal stability of zeolitic imidazolate frameworks. *Proceedings of the National Academy of Sciences of the United States of America* **2006,** *103* (27), 10186-91.

63. Wang, B.; Cote, A. P.; Furukawa, H.; O'Keeffe, M.; Yaghi, O. M., Colossal cages in zeolitic imidazolate frameworks as selective carbon dioxide reservoirs. *Nature* **2008,** *453* (7192), 207-11.

64. (a) Vogels, L. J. P.; van Hoof, P. J. C. M.; Grimbergen, R. F. P., On the roughening transition of anisotropic and (pseudo) hexagonal lattices. *Journal of Crystal Growth* **1998,** *191* (3), 563-572; (b) Ge, L.; Zhou, W.; Du, A.; Zhu, Z., Porous Polyethersulfone-Supported Zeolitic Imidazolate Framework Membranes for Hydrogen Separation. *The Journal of Physical Chemistry C* **2012,** *116* (24), 13264-13270.

65. Liang, Z.; Marshall, M.; Chaffee, A. L., CO2 Adsorption-Based Separation by Metal Organic Framework (Cu-BTC) versus Zeolite (13X). *Energy & Fuels* **2009,** *23* (5), 2785-2789.

66. Zhang, K.; Nalaparaju, A.; Chen, Y.; Jiang, J., Crucial role of blocking inaccessible cages in the simulation of gas adsorption in a paddle-wheel metal–organic framework. *RSC Advances* **2013,** *3* (36), 16152.

67. Choi, E.-Y.; Barron, P. M.; Novotny, R. W.; Son, H.-T.; Hu, C.; Choe, W., Pillared Porphyrin Homologous Series: Intergrowth in Metal–Organic Frameworks. *Inorganic chemistry* **2009,** *48* (2), 426-428.

68. (a) Zhang, L.; Zhuo, Y.; Du, W.; Tao, Y.; Chen, C.; Xu, X., Hg Removal Characteristics of Noncarbon Sorbents in a Fixed-Bed Reactor. *Industrial & Engineering Chemistry Research* **2012,** *51* (14), 5292-5298; (b) Pavlish, J. H.; Sondreal, E. A.; Mann, M. D.; Olson, E. S.; Galbreath, K. C.; Laudal, D. L.; Benson, S. A., Status review of mercury control options for coal-fired power plants. *Fuel Processing Technology* **2003,** *82* (2-3), 89-165.

69. Frahm, D.; Hoffmann, F.; Fröba, M., Two Metal–Organic Frameworks with a Tetratopic Linker: Solvent-Dependent Polymorphism and Postsynthetic Bromination. *Crystal Growth & Design* **2014,** *14* (4), 1719-1725.

70. Göbel, M.; Tchitchanov, B. H.; Murray, J. S.; Politzer, P.; Klapötke, T. M., Chlorotrinitromethane and its exceptionally short carbon–chlorine bond. *Nature chemistry* **2009,** *1* (3), 229-235.

71. Clark, T.; Hennemann, M.; Murray, J.; Politzer, P., Halogen bonding: the σ-hole. *Journal of molecular modeling* **2007,** *13* (2), 291-296.

72. Wiley, D. W.; Webster, O. W.; Blanchard, E. P., Hydrogen cyanide chemistry. 6. Cyanogen condensation with cyanide, C7N7. *The Journal of Organic Chemistry* **1976,** *41* (11), 1889-1895.

73. Su, C.-Y.; Goforth, A. M.; Smith, M. D.; Pellechia, P. J.; zur Loye, H.-C., Exceptionally Stable, Hollow Tubular Metal−Organic Architectures: Synthesis, Characterization, and Solid-State Transformation Study. *Journal of the American Chemical Society* **2004,** *126* (11), 3576-3586.

74. Zheng, Y.-Z.; Zhang, Y.-B.; Tong, M.-L.; Xue, W.; Chen, X.-M., Syntheses, structures and magnetic properties of a family of metal carboxylate polymersviain situ metal-ligand reactions of benzene-1,2,3-tricarboxylic acid. *Dalton transactions* **2009,** (8), 1396-1406.

75. Liu, X.; Pan, S.; Wu, J.; Wang, Y.; Chen, W., A Planar π-Conjugated Naphthyridine-Based N-Heterocyclic Carbene Ligand and Its Derived Transition-Metal Complexes. *Organometallics* **2012,** *32* (1), 209-217.

76. Li, J.; Brill, T. B., Spectroscopy of Hydrothermal Reactions 20: Experimental and DFT Computational Comparison of Decarboxylation of Dicarboxylic Acids Connected by Single, Double, and Triple Bonds. *The Journal of Physical Chemistry A* **2002,** *106* (41), 9491-9498.

77. Chen, W.; Wang, J.-Y.; Chen, C.; Yue, Q.; Yuan, H.-M.; Chen, J.-S.; Wang, S.-N., Photoluminescent Metal−Organic Polymer Constructed from Trimetallic Clusters and Mixed Carboxylates. *Inorganic chemistry* **2003,** *42* (4), 944-946.

78. Fang, Q.; Zhu, G.; Shi, X.; Wu, G.; Tian, G.; Wang, R.; Qiu, S., Synthesis, structure and fluorescence of a novel three-dimensional inorganic–organic hybrid

polymer constructed from trimetallic clusters and mixed carboxylate ligands. *Journal of Solid State Chemistry* **2004,** *177* (4-5), 1060-1066.

79. Ouellette, W.; Prosvirin, A. V.; Chieffo, V.; Dunbar, K. R.; Hudson, B.; Zubieta, J., Solid-State Coordination Chemistry of the Cu/Triazolate/X System (X = F-, Cl-, Br-, I-, OH-, and SO42-). *Inorganic chemistry* **2006,** *45* (23), 9346-9366.

80. Chesnut, D. J.; Kusnetzow, A.; Birge, R.; Zubieta, J., Ligand Influences on Copper Cyanide Solid-State Architecture: Flattened and Fused "Slinky", Corrugated Sheet, and Ribbon Motifs in the Copper−Cyanide−Triazolate−Organoamine Family. *Inorganic chemistry* **1999,** *38* (24), 5484-5494.

81. Park, H.; Krigsfeld, G.; Teat, S. J.; Parise, J. B., Synthesis and Structural Determination of Four Novel Metal−Organic Frameworks in a Zn−3-Amino-1,2,4-Triazole System. *Crystal Growth & Design* **2007,** *7* (7), 1343-1349.

82. (a) Devic, T.; Horcajada, P.; Serre, C.; Salles, F.; Maurin, G.; Moulin, B.; Heurtaux, D.; Clet, G.; Vimont, A.; Grenèche, J.-M.; Ouay, B. L.; Moreau, F.; Magnier, E.; Filinchuk, Y.; Marrot, J.; Lavalley, J.-C.; Daturi, M.; Férey, G., Functionalization in Flexible Porous Solids: Effects on the Pore Opening and the Host−Guest Interactions. *Journal of the American Chemical Society* **2009,** *132* (3), 1127-1136; (b) Barthelet, K.; Marrot, J.; Riou, D.; Férey, G., A Breathing Hybrid Organic–Inorganic Solid with Very Large Pores and High Magnetic Characteristics. *Angewandte Chemie International Edition* **2002,** *41* (2), 281-284; (c) Zhao, Y.; Seredych, M.; Zhong, Q.; Bandosz, T. J., Aminated graphite oxides and their composites with copper-based metal-organic framework: in search for efficient media for CO2 sequestration. *RSC Advances* **2013,** *3* (25), 9932-9941.

83. Chen, K.-J.; Lin, R.-B.; Liao, P.-Q.; He, C.-T.; Lin, J.-B.; Xue, W.; Zhang, Y.-B.; Zhang, J.-P.; Chen, X.-M., New Zn-Aminotriazolate-Dicarboxylate Frameworks: Synthesis, Structures, and Adsorption Properties. *Crystal Growth & Design* **2013,** *13* (5), 2118-2123.

84. Bordiga, S.; Lamberti, C.; Ricchiardi, G.; Regli, L.; Bonino, F.; Damin, A.; Lillerud, K. P.; Bjorgen, M.; Zecchina, A., Electronic and vibrational properties of a MOF-5 metal-organic framework: ZnO quantum dot behaviour. *Chemical communications* **2004,** (20), 2300-2301.

CURRICULUM VITAE

Articles in peer-reviewed journals

1 Liu, Xin; Valentine, Haley, L; Pan, Wei-Ping; Cao, Yan; Yan, Bangbo; Two new porous 2D metal-organic frameworks: synthesis and structures **2015**. (Manuscript Submitted to *CrystEngComm.*)

2 Bangbo Yan; Xin Liu; Tushar Ghugare; Nicholas Fedorka; Yan-Fem Li, 2D Metalloporphyrin Coordination Network of Cobalt-meso-tetra (4-carboxyphenyl) porphyrin **2015**. (Manuscript Submitted to *Coordination Chemistry.*)

3 Bangbo Yan; Raj Kishore Vakiti; Nicholas Fedorka; Xin, Liu; Yan Cao; Wei-Ping Pan,3-D Metal-organic Frameworks Based On S-Block Metal Ions. *Inorganica Chimica Acta* **2014**, *421*, 544-548

Presentations at academic conferences

1 Liu Xin; Fedorka, Nicholas; Yan Bangbo. "Development of MOFs Material for Mercury Removal" Kentucky Academy of Science, Lexington, KY, USA, 2014

2 Liu Xin; Fedorka, Nicholas; Yan Bangbo. "Novel Porous Materials for Mercury Removal" SERMACS, Nashville, TN, USA, 2014.

3 Brady D. Garabato, Xin Liu, Yan Bangbo. "Heteronuclear Niobium-Lanthanide Oxo Clusters: Syntheses, Structures and Properties" 2013 KY EPSCoR Annual Conference, Louisville, KY, USA, 2013

ABBREVIATIONS AND SYMBOLS

Htrz	1,2,4-trizaole
MeIM	2-methylimidazole
BTC	Benzene 1,3,5-tricarboxylic acid
BrBDC	2,5-dibromoterepthalic acid
DMF	N,N-Dimethylformamide
TEA	trimethylamine
BET	Brunauer-Emmett-Teller surface area
XRD	X-Ray Diffraction
PXRD	Powder X-Ray Diffraction
SEM	Scanning electron microscope
TEM	Transmission electron microscope